Sandstone body character and river planform styles of the lower Eocene Willwood Formation, Bighorn Basin, Wyoming, USA

Wang, Youwei; Baars, Timothy F.; Sahoo, Hiranya; Storms, Joep E.A.; Martinius, Allard W.; Gingerich, Philip; Abels, Hemmo A.

DOI
10.1111/sed.13027

Publication date
2022

Document Version
Final published version

Published in
Sedimentology

Citation (APA)
Wang, Y., Baars, T. F., Sahoo, H., Storms, J. E. A., Martinius, A. W., Gingerich, P., & Abels, H. A. (2022). Sandstone body character and river planform styles of the lower Eocene Willwood Formation, Bighorn Basin, Wyoming, USA. *Sedimentology*, *69*(7), 2897-2924. https://doi.org/10.1111/sed.13027

SEDIMENTOLOGY the journal of the International Association of Sedimentologists

Sedimentology (2022) **69**, 2897–2924 doi: 10.1111/sed.13027

Sandstone body character and river planform styles of the lower Eocene Willwood Formation, Bighorn Basin, Wyoming, USA

YOUWEI WANG*,[1], TIMOTHY F. BAARS*, HIRANYA SAHOO*, JOEP E. A. STORMS*, ALLARD W. MARTINIUS*†, PHILIP GINGERICH‡ and HEMMO A. ABELS*

**Department of Geosciences and Engineering, Delft University of Technology, Stevinweg 1, Delft, 2628 CN, The Netherlands (E-mail: youweiwang2021@outlook.com)*

†Equinor ASA, Arkitekt Ebbellsvei 10, N-7053, Trondheim, Norway

‡Museum of Palaeontology, University of Michigan, Ann Arbor, MI, 48109-1079, USA

Associate Editor – Christopher Fielding

ABSTRACT

The lower Eocene Willwood Formation of the Bighorn Basin, Wyoming, USA, is an alluvial succession with a sand content varying around 25%. It has been studied intensively for palaeontology, palaeoenvironments and palaeoclimates, as well as sedimentological and stratigraphic analysis. Channel dynamics were studied at a relatively low resolution throughout the basin over the geological time from late Palaeocene to early Eocene. Here, a high-resolution study is reported to complement previous research at the basin scale. Efforts are made to document the characteristics and river planform styles of most sandstone bodies encountered through *ca* 300 m of alluvial stratigraphy in a 10 km^2 area of the Deer Creek part of the McCullough Peaks area situated in the basin axis of northern Bighorn Basin. Four channel facies associations are recognized and ascribed to four river planform styles: crevasse channel, trunk channel, braided-like channel and sinuous-like channel, with the latter two types dominant. Braided-like and sinuous-like channel sandstone bodies differ significantly in thicknesses, being on average 6.1 m versus 9.0 m, but they have similar palaeoflow–perpendicular widths of on average 231 m and palaeoflow directions of on average N 003°. Braided-like and sinuous-like river planform styles show no spatial dependency in the 10 km^2 study area. Results of this study are in line with existing basin-scale depositional models that are composed of a single axial system fed by several transverse systems dominantly from the west. The feeding of these systems could be influenced by palaeoclimate changes possibly controlling their contribution over time, thereby impacting river planform styles. At the same time, changing water discharge hydrograph, sediment load and overbank cohesiveness may have equally driven the observed river planform style changes within the basin without a major role of catchments.

Keywords Bighorn Basin, channel sandstone body, palaeogeography, river planform style, Willwood Formation.

[1]Present address: Department of Environmental Sciences, University of Virginia, Charlottesville, VA, 22903, USA

INTRODUCTION

Alluvial architecture illustrates the size, shape and spatial arrangement of fluvial channel bodies and their associated facies in three dimensions (Allen, 1978; Bridge & Leeder, 1979). The architecture is controlled by both autogenic processes, such as channel avulsion and self-organization (e.g. Mackey & Bridge, 1995; Hajek *et al.*, 2010), and allogenic factors, such as climate, basin subsidence and uplifting, and base level (e.g. Shanley & McCabe, 1994; Holbrook *et al.*, 2006; Hampson *et al.*, 2013; Bijkerk *et al.*, 2014). Extensive studies have been conducted on alluvial deposits using various approaches and datasets, including high-resolution three-dimensional seismic data (e.g. Posamentier *et al.*, 2007), numerical modelling (e.g. Jerolmack & Paola, 2007; Karssenberg & Bridge, 2008; Wang *et al.*, 2021) and outcrop analogues (e.g. Fielding, 1986, 2006; Allen *et al.*, 2013; Colombera *et al.*, 2016, 2017; Ghinassi *et al.*, 2016; Ghinassi & Ielpi, 2018). Outcrops provide data that span large hierarchical temporal and spatial scales, which can help interpret depositional environments, reconstruct palaeoclimates (e.g. Howell *et al.*, 2014; Colombera *et al.*, 2016; Paredes *et al.*, 2016) and build subsurface predictive models (e.g. Bryant *et al.*, 2000; Enge *et al.*, 2007).

By investigating alluvial strata in the Bighorn Basin, Wyoming, USA, numerous studies have reported on a variety of aspects: for example, palaeontology (Gingerich, 2010); palaeomagnetism (Clyde *et al.*, 1994); palaeosols (Bown & Kraus, 1981; Kraus & Gwinn, 1997; Davies-Vollum, 1999, 2001; Kraus, 1999, 2002; Abels *et al.*, 2013; Wang *et al.*, 2021); and channel sandstone bodies – the focus of this study (van Houten, 1944; Neasham, 1970; Neasham & Vondra, 1972; Kraus & Middleton, 1987; Bown & Kraus, 1987; Kraus, 1985, 1996; Willis & Behrensmeyer, 1995; Kraus & Gwinn, 1997; Kraus & Wells, 1999; Davies-Vollum & Kraus, 2001; Clyde & Christensen, 2003; Kraus & Davies-Vollum, 2004; Foreman, 2014; Owen *et al.*, 2017). The well-documented floodplain cyclicity in the Willwood Formation of the Bighorn Basin provides an opportunity to investigate the influence of orbital climate forcing on alluvial architecture (Abdul Aziz *et al.*, 2008; Abels *et al.*, 2013; Wang *et al.*, 2021). Also, extreme climate warming has been observed to impact alluvial architecture in the basin (Foreman, 2014; van der Meulen *et al.*, 2020).

Generic relationships between channel and floodplain deposits were illustrated over basin scales, with thick sheet sandstones ascribed to meandering river processes (Kraus & Middleton, 1987; Kraus & Gwinn, 1997; Foreman, 2014). Moreover, the Bighorn Basin is suggested to host an axial river system and several transverse systems (Kraus & Middleton, 1987; Owen *et al.*, 2019). Interaction between these systems could have influenced the geomorphology downstream of the interfingering sites. This hypothesis has been corroborated by data of Owen *et al.* (2019) analysing the downstream variation trends of channel proportion and geometry as well as grain size. The channel sandstone bodies studied in Owen *et al.* (2019) are spread through the basin and of different stratigraphic levels. In this context, documentation of all sandstone bodies in one continuous succession in a single area could aid the understanding of changes of fluvial dynamics in space and time, further document the possible interaction between the axial and transverse systems, and validate or refine existing depositional models.

In this study, efforts are therefore made to investigate the lower Eocene channel sandstone bodies in the Deer Creek portion of the McCullough Peaks area of the northern Bighorn Basin situated in the proximity of the basin axis (Fig. 1; Kraus & Middleton, 1987). Sandstone bodies that occur in *ca* 300 m of stratigraphy are targeted to analyse their geometry and internal characteristics, reconstruct their related river planform styles, and interpret their character within the frame of the basin-scale geomorphology. This is done by combining field documentation with observations in a georeferenced photogrammetric model developed using an unmanned aerial vehicle (UAV) in a 10 km^2 area.

GEOLOGICAL BACKGROUND

Structural setting, tectonics and provenance

The Bighorn Basin is a Laramide intermontane basin in north-western Wyoming within the Western Interior of the United States with a length of *ca* 200 km and a width of *ca* 80 km (Kraus & Middleton, 1987; Fig. 1). It was bounded by the western Beartooth Mountains, south-western Washakie Range, eastern Bighorn Mountains and the north-eastern Pryor

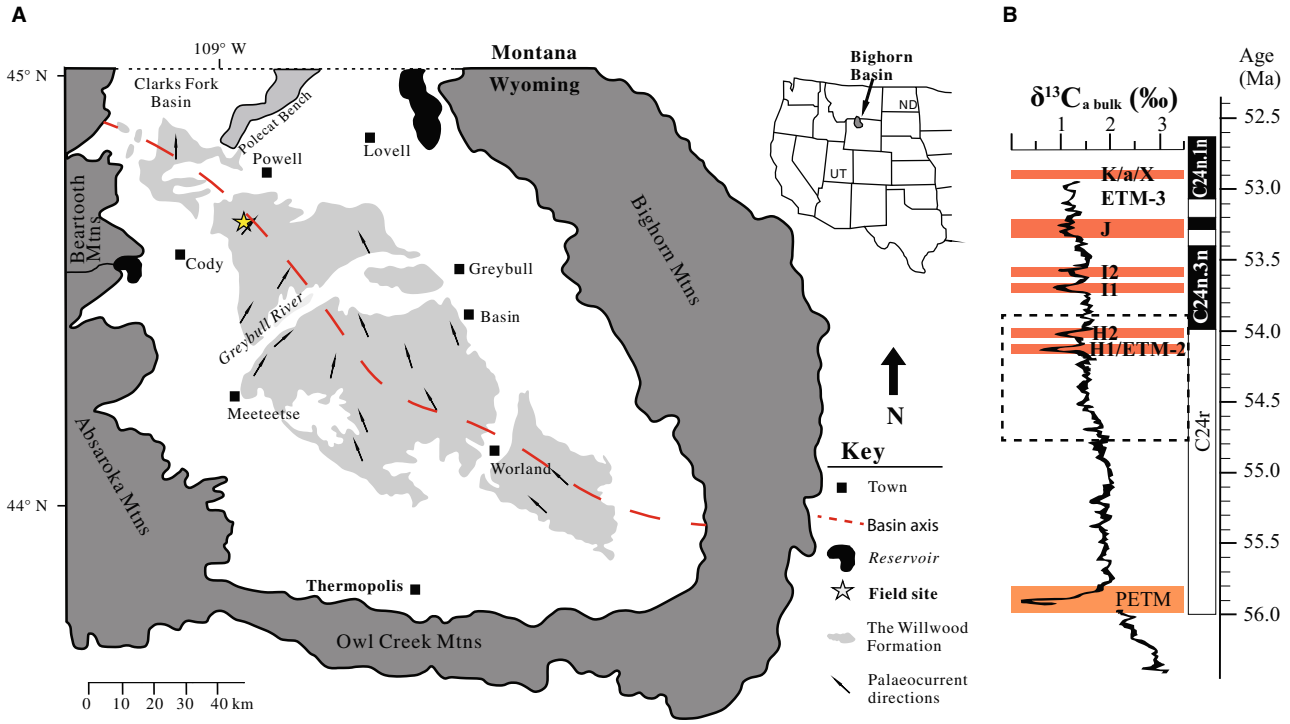

Fig. 1. (A) The location of the study area, the McCullough Peaks, in the northern Bighorn Basin, Wyoming, USA (after Wang *et al.*, 2017), with the yellow pentagram between Cody and Powell indicating its position. The basin axis follows Finn *et al.* (2010) and the palaeocurrent data are from Neasham & Vondra (1972). Note that the Washakie Range present during the Eocene is now covered by the Absaroka Mountains (Yonkee & Weil, 2015) and the Pryor Mountains present during the Eocene are now not distinguishable from the Bighorn Mountains (Blackstone, 1940). (B) Adjusted $\delta^{13}C_{a\ bulk}$ data from Zachos *et al.* (2010) to Gradstein *et al.* (2012) global timescale (Vandenberghe *et al.*, 2012) by Birgenheier *et al.* (2019), with orange rectangles indicating hyperthermal events and the dashed rectangle indicating the study interval. ETM = Eocene Thermal Maximum in part (B).

Mountains from Palaeocene to Early Eocene (Foose *et al.*, 1961; Lillegraven & Ostresh Jr., 1988). The Absaroka Range was formed by volcanic activity during the late early and middle Eocene (Smedes & Prostka, 1972), which makes it challenging to constrain the south-western margin of the Bighorn Basin in the Eocene. The eastern margin of the basin has always had a relatively gentle slope (Yonkee & Weil, 2015). Neasham & Vondra (1972) suggested most Willwood sandstone units to be subarkose, with a mainly western source. In contrast, Kraus & Middleton (1987) indicated that most sandstone bodies in their study area (the Clarks Fork Basin in front of the Beartooth Range) are litharenites, with the main source area in the Beartooth Mountains. Other work indicates the presence of multiple provenances, including all of the mountainous areas expressed before or during the early Eocene (e.g. Owen *et al.*, 2019).

Beartooth Mountains to the north-west

The major uplift of the Beartooth Mountains took place during the mid to late Palaeocene (Gingerich, 1983). The eastern flank of the Beartooth Mountains was very steep, with *ca* 8000 m of structural relief (Wise, 2000). According to the work by DeCelles *et al.* (1991), the Beartooth fluvial systems are composed of several ephemeral coarse-grained alluvial fans and braid-plain deposits, although these are Palaeocene in age and thus older than our studied stratigraphic interval. Lacustrine deposits are reported in the north-west of Powell, in the mountain front close to the Polecat Bench area (Fig. 1; Yuretich *et al.*, 1984).

Absaroka Mountains to the west

The Absaroka Mountains forming the western margin of the present-day Bighorn Basin were not emplaced until near the end of Willwood Formation deposition, since volcanic activity started in the middle early to middle Eocene

(Smedes & Prostka, 1972; Sundell, 1990). This makes it challenging to understand the original catchment of the Bighorn Basin fluvial system. Extensive discussion on this has been presented in Owen *et al.* (2019), where the authors summarized several different source areas to the west that have been proposed in the literature, including the Cody Arch by van Houten (1944) and Sundell (1990) and the Washakie Range by Lillegraven (2009) and Kraus (1985).

Washakie Range to the west/south-west

It is suggested that the Washakie Range, present during the Palaeocene and early Eocene, was located farther west of the current western basin boundary, with a steep front towards the east (van Houten, 1944; Kraus, 1983, 1985; Sundell, 1990; Lillegraven, 2009). Overthrusting associated with the formation of the mountain range is likely to have influenced the development of the Willwood sedimentary sequences (Yonkee & Weil, 2015), thus making it difficult to constrain the characteristics of the fluvial system fed by this source terrain. According to Owen *et al.* (2019), at the time the Willwood system was active, it was characterized as a distributive fluvial system, with conglomeratic input from the Washakie Range. Kraus (1984) reported early Eocene fanglomerates in the alluvial fan system sourcing from this range. Based on their detrital zircon geochronology of quartzite clasts, Malone *et al.* (2017) and Syzdek *et al.* (2019) provided additional hypotheses for the provenance of fluvial systems to the west closer to the Sevier thrust belt (see the Willwood conglomerates at Meeteetse in fig. 2 of Malone *et al.*, 2017).

Owl Creek Mountains to the south

The uplift around the southern margin of the basin formed the southern Bighorn and Owl Creek Mountains, which were subsequently thrust southward in the early–mid Eocene (Wing & Bown, 1985). In general, major reverse thrusts verged to the south in the Owl Creek Mountains (Gries, 1983), and thus the northern slope of the Owl Creek Mountains was gentle (not steeply faulted) during the early Eocene, and the southern part of the Bighorn Basin was relatively low, probably only forming a gentle rise separating the Bighorn Basin from the Powder River Basin in the south (Wing & Bown, 1985).

Bighorn Mountains to the south-east and east

The Bighorn Mountains have a long shallowly dipping slope on the Bighorn Basin side and a steep thrust scarp on the Powder River Basin side (Hoy & Ridgway, 1997; Yonkee & Weil, 2015). Swampy and lacustrine deposits are indicated to be present in front of the Bighorn Mountains on the Bighorn Basin side (Wing & Bown, 1985; Davies-Vollum & Wing, 1998). There might be a sizeable contribution of sediment from the Bighorn Mountains to the easternmost basinfill, but comparatively less sediment would influence the McCullough Peaks study area given the presence of several progressive unconformities in between and the relatively gentle gradient. Westerly palaeocurrents are rarely documented in the eastern and south-eastern parts of the basin (Owen *et al.*, 2019), suggesting that the eastern side of the basin might have contributed little to the basin fill.

Pryor Mountains to the north-east

The Pryor Mountains are interpreted to be asymmetrical anticlines that experienced overthrusting in the later stages (Blackstone, 1940). They are not considered an important sediment source (Wilson, 1936; Seeland, 1998; Owen *et al.*, 2019) nor a consistent drainage barrier (Dickinson *et al.*, 1988). There was a 'Pryor Gap' between the Pryor Mountains and the Bighorn Mountains (see fig. 2 in Blackstone, 1940), which could have served as a possible exit for the fluvial system during the deposition of the Willwood Formation (Dickinson *et al.*, 1988; Owen *et al.*, 2019).

Early Eocene climate and Willwood Formation deposition

The global early Eocene is indicated to be in a hothouse state, with a globally average temperature *ca* 12°C higher than the present global average (Westerhold *et al.*, 2020; Scotese *et al.*, 2021). The early Eocene Bighorn Basin is suggested to have been in a warm-temperate to subtropical environment with seasonal precipitation (van Houten, 1944). The basin landscape may resemble modern-day savannahs, with broad open areas interspersed with forest-bordering streams (Neasham, 1967). In the meantime, it is alternatively suggested to be like canopy-structure woodlands by Secord *et al.* (2008). Two hyperthermal events are recorded in the upper part of the study interval, referred to as H1/ETM2 and H2 (Abels *et al.*, 2012; Fig. 1).

The lower Eocene Willwood Formation consists of a series of alluvial deposits that are

currently exposed in the central part of the basin roughly along the NNW–SSE-extending basin axis (Fig. 1). It is mainly composed of sandstones, siltstones and claystones, parts of which have undergone intensive pedogenic modification (Kraus & Davies-Vollum, 2004). Extensive studies have been carried out, with the main focus on palaeosols (Kraus, 1999, 2002), processes of river avulsion (Neasham & Vondra, 1972; Kraus & Gwinn, 1997; Kraus & Davies-Vollum, 2004), fluvial sedimentology (Kraus & Middleton, 1987; Willis & Behrensmeyer, 1995; Kraus & Gwinn, 1997; Kraus, 2002; Owen *et al.*, 2017, 2019) and fluvial cyclicity (Clyde & Christensen, 2003; Abdul Aziz *et al.*, 2008; Abels *et al.*, 2013; van der Meulen *et al.*, 2020; Wang *et al.*, 2021). The dominant palaeoflow direction is interpreted to be NNW to NNE during the late Palaeocene and early Eocene (Neasham & Vondra, 1972; Kraus, 1980; Kraus & Middleton, 1987; Seeland, 1998; Foreman, 2014; Owen *et al.*, 2017, 2019; Wang *et al.*, 2021), thus approximately paralleling the trend of the basin axis (Kraus & Middleton, 1987; Finn *et al.*, 2010). Cyclic palaeosol maturation patterns associated with heterolithic avulsion deposits have been inferred as the result of allogenic forcing (Kraus & Aslan, 1993; Abdul Aziz *et al.*, 2008; Abels *et al.*, 2013; Van der Meulen *et al.*, 2020; Wang *et al.*, 2021). The sediment accumulation rate estimated by various studies ranges between 288 m and 391 m Myr^{-1} (Clyde *et al.*, 1994; Gingerich, 2010; Abels *et al.*, 2013, 2016; Wang *et al.*, 2021).

Channel sandstone bodies are classified into two main categories that are spatiotemporally dispersed unevenly across the basin, namely sheet-type and ribbon-type sandstone bodies (van Houten, 1944; Kraus, 1985, 2002; Kraus & Middleton, 1987; Kraus & Gwinn, 1997). In terms of their origin, ribbon-type sandstone bodies are interpreted to represent a distributary fluvial network linked to the process of avulsion (Kraus, 1985, 2002; Kraus & Middleton, 1987; Kraus & Gwinn, 1997), while sheet-type sandstone bodies are interpreted as the product of the possibly present axial river system (Kraus & Middleton, 1987; Seeland, 1998; Foreman, 2014). More recently, Owen *et al.* (2017) subdivided the sheet geometry into five types, including the massive channel body geometry, semi-amalgamated channel body geometry, internally amalgamated channel body geometry, offset stacked channel body geometry and isolated channel body geometry. Owen *et al.* (2019) linked the complex nature of the Bighorn Basin fill to the component depositional systems with a relatively wide axial system and several transverse distributive fluvial systems by systematically analysing the downstream trends of channel percentage and geometry as well as grain size. River planforms that contribute to the fluvial deposits in the Bighorn Basin are thought to mainly include sinuous rivers and braided rivers (e.g. van Houten, 1944; Bown & Kraus, 1981, 1987; Kraus, 1985, 2002; DeCelles *et al.*, 1991; Willis & Behrensmeyer, 1995; Kraus & Wells, 1999; Davies-Vollum & Kraus, 2001; Kraus & Davies-Vollum, 2004; Foreman, 2014; Owen *et al.*, 2017, 2019).

DATASET AND METHODOLOGY

Fieldsite documentation

Sandstone bodies were systematically documented in the field (Fig. 2) using a standard set of parameters including grain size, lithology, sedimentary structure, geometry, boundaries, palaeo-flow directions and dimensions. Based on these documentations, lithofacies and lithofacies association classification schemes are established following methods outlined by Allen (1983) and Miall (1985, 1996). Data were collected structurally with spreadsheets and short sedimentary logs to characterize each sandstone body type. The grain size was measured by observing the grains together with a grain-size chart under a hand lens. Dimensions of sandstone bodies were measured using Jacob's staff, flexible tapes and a laser rangefinder when not directly accessible. The colour was described according to the methods detailed in the Soil Survey Manual (Soil Survey Division Staff, 1993). Palaeocurrent data and cross-set thickness were measured from dune-scale cross-stratification (mainly planar and trough cross-stratification).

Unmanned aerial vehicle-based photogrammetry

The preparation of the UAV-based photogrammetric model has been detailed in Wang *et al.* (2021). The model includes 21 144 photographs taken on 34 flights and it covers a total area of *ca* 10 km^2, with approximate north–south and east–west lengths of 2.5 km and

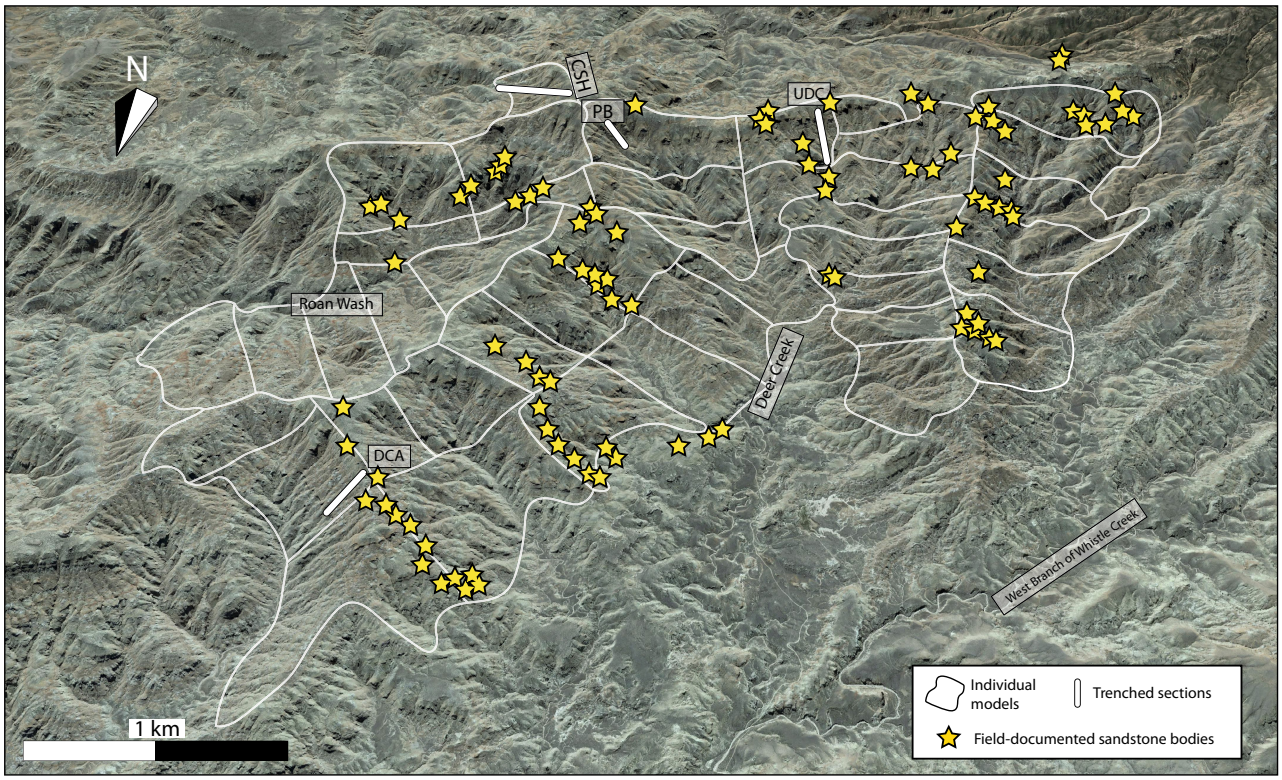

Fig. 2. Bird's eye view from Google Earth© showing unmanned aerial vehicle (UAV)-based photogrammetric model coverage and field-documented sandstone bodies in the McCullough Peaks area (see its position in Fig. 1). Abbreviations: DCA, Deer Creek Amphitheatre section (Abels *et al.*, 2013); UDC, Upper Deer Creek section (Abels *et al.*, 2012); CSH, Creek Star Hill section (Abels *et al.*, 2016); and PB, Purple Butte section.

4.0 km, respectively. The studied stratigraphic succession is *ca* 300 m thick and dips at *ca* 2° towards the south. Fifty-seven ground control points (GCPs) were placed, contributing to centimetre accuracy relative to the local base station. Agisoft PhotoScan (Version 1.4.3, July 2018; current Metashape) was used to build the three-dimensional digital models, which were later imported into LIME (version 2.2.2; Buckley *et al.*, 2019) for visualization and interpretation.

Petrological analysis

A total of 32 sandstone samples was collected from outcrops in the study area and made into thin sections in the laboratory. Classification of sandstones follows the scheme by Mcbride (1963) that groups framework grains into: (i) quartz plus chert and quartzite; (ii) feldspar; and (iii) rock fragments and accessory minerals. It should be noted here that the specimen sampling is biased in terms of the specimen number during the field work when types of deposits were not identified yet. Therefore, it appeared that specimens of some types were more collected than others. Covid-19 travel restrictions prevented further sampling in 2020 and 2021.

Formative bankfull depth estimation

Dune-scale cross-set thickness (S_m) has been used empirically to estimate the mean formative bedform height (h_m), as is shown in Eq. 1 (Bridge & Tye, 2000; Leclair & Bridge, 2001). The application of this method requires meeting the precondition that the coefficient of variation (ratio of standard deviation to mean) of the preserved cross-set thickness should vary between 0.58 and 1.18 (Bridge & Tye, 2000).

$$h_m = 2.9\ (\pm 0.7)\ S_m \quad (1)$$

Then, the mean formative bankfull depth (d) can be estimated based on the empirical equation proposed by Bradley & Venditti (2017):

$$d = 6.7\ h_m \text{ (with 50\% prediction interval : 4.4 } h_m \text{ to 10.1 } h_m) \quad (2)$$

Statistical analysis

Two-sample *t*-tests are performed to assess whether there are statistically significant differences between different types of deposits in terms of channel sandstone body thickness and width. Palaeocurrent data are analysed as circular data using the R programming language, and the Rayleigh Test of Uniformity is implemented to check whether the distribution of the palaeoflow data of certain deposits is significantly different from the uniform distribution. Watson's Two-Sample Test of Homogeneity is employed to compare whether the distributions of the palaeoflow data of two types of channel deposits are significantly different from one another.

RESULTS

Lithofacies analysis

Based on detailed observation and description of grain size, lithology, internal sedimentary structures and spatial positions in the sandstone bodies, a total of 12 lithofacies are recognized in the field (Fig. 3 and Table 1). There are one conglomeratic lithofacies, named clast-supported conglomerate (G); nine sandy lithofacies, including massive sandstone (Sm), trough cross-stratified sandstone (St), planar/tabular cross-stratified sandstone (Sp), ripple cross-laminated sandstone (Sr), climbing-ripple cross-laminated sandstone (Scr), low-angle (<15°) cross-stratified sandstone (Sl), sandstone with erosional scour and fill (Se), bioturbated sandstone (Sb) and convoluted sandstone (Sc); and two silty to muddy lithofacies: mudstones and siltstones (Fs) and laminated siltstones (Fl). Details of their character and interpretation are given in Table 1.

Facies association analysis

According to the organizations of lithofacies in the vertical succession and lateral distribution (Table S1), a total of five sandy facies associations are classified, which fall into two major categories, namely channel facies associations and floodplain facies associations.

Channel facies associations

Facies Association 1 – Small-scale crevasse channel sandstone deposits

Description: Facies Association 1 (FA1) is mainly composed of fine to medium-grained sandstone bodies, with a thickness range of 0.5 to 3.0 m and an average of 1.9 m ($n = 15$). Its indurated part shows a lenticular external geometry with concave-up margins in the transverse view (Fig. 4A) and ribbon-shaped geometry in the longitudinal view (Fig. 4B). Various lithofacies are present, including trough cross-stratified sandstone (St), planar/tabular cross-stratified sandstone (Sp) and ripple cross-laminated sandstone (Sr). Within FA1, trough cross-stratified sandstone (St), if present, is usually in the lower part, planar/tabular cross-stratified sandstone (Sp) in the middle part, and ripple cross-laminated sandstone (Sr) in the upper part. This facies association is generally encased within floodplain deposits that present pedogenic features due to subaerial exposure. The contact between FA1 and floodplain fines is usually sharp with floodplain fines passively draping the top of the sandstone body.

Interpretation: FA1 is interpreted to be the product of straight crevasse channels (Kraus & Gwinn, 1997; Clyde & Christensen, 2003; Gibling, 2006), also known as feeder channels of the avulsion complex (*cf.* Davies-Vollum & Kraus, 2001). The sharp contact with floodplain fines indicates an erosional base, the massive structure indicates rapid cut-and-fill processes, and the presence of cross-bedding suggests downstream traction of stream power. Similarly, at localities in the vicinity of the study area, FA1 is reported to be generally thinner than 3 m (Clyde & Christensen, 2003) and referred to as ribbon sandstone bodies (Kraus & Middleton, 1987). In this study, all of the FA1 sandstone bodies were observed to occur in isolation, while they can also be nested/stacked, as demonstrated by Davies-Vollum & Kraus (2001) who describe the geometry and architecture of these in detail in the central part of the Bighorn Basin.

Facies Association 2 — Large-scale trunk channel sandstone deposits

Description: Facies Association 2 (FA2) is mainly composed of fine to medium-grained sandstone (Fig. 5), with a thickness range of 8 to 15 m and an average of 9.8 m ($n = 5$). FA2

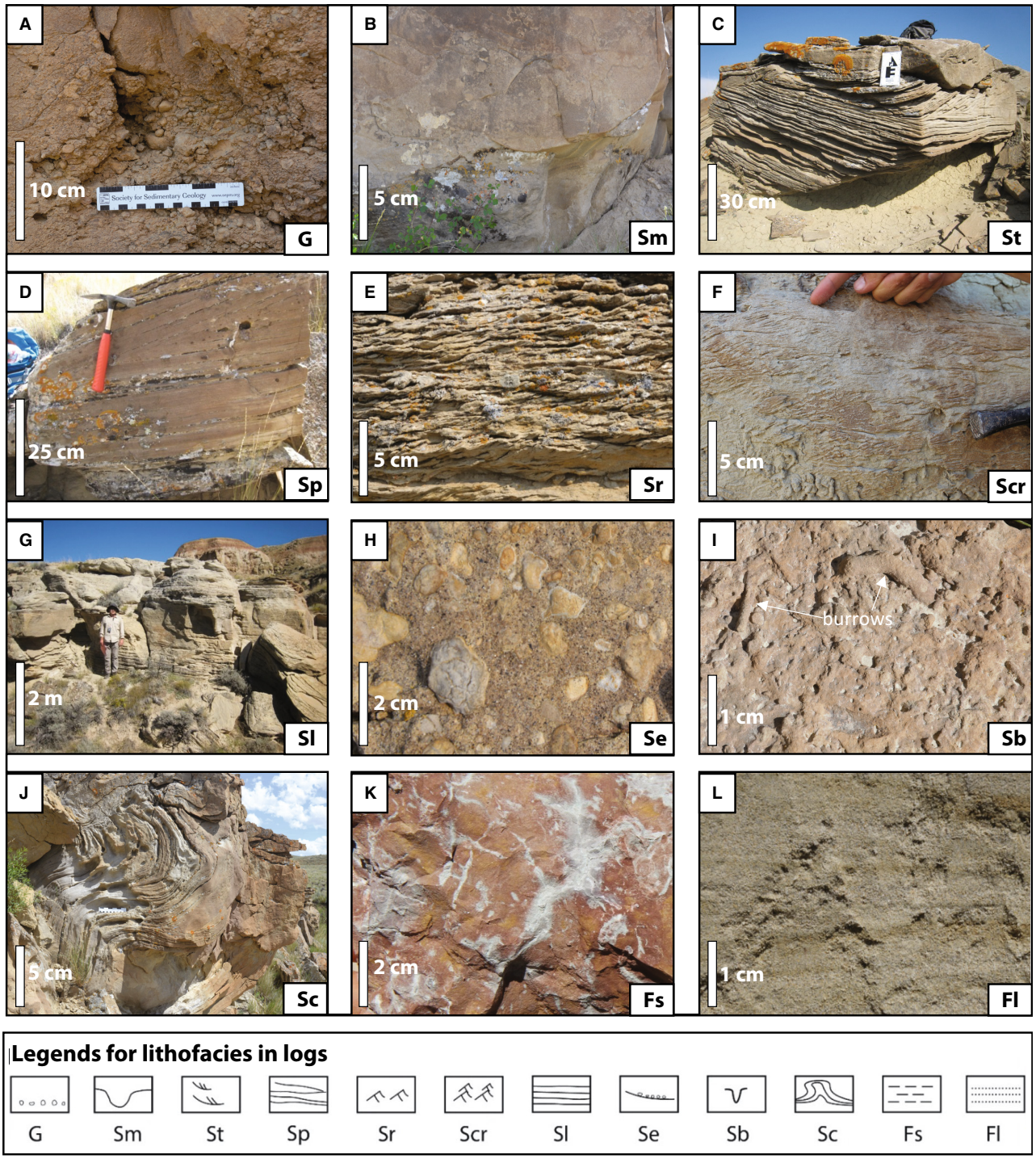

Fig. 3. Lithofacies recognized in the study area. (A) Clast-supported conglomerate (lithofacies G). (B) Massive sandstone (lithofacies Sm). (C) Trough cross-stratified sandstone (lithofacies St). (D) Planar/Tabular cross-stratified sandstone (lithofacies Sp); hammer length = 25 cm. (E) Ripple cross-laminated sandstone (lithofacies Sr). (F) Climbing-ripple cross-laminated sandstone (lithofacies Scr). (G) Low-angle (<15°) cross-bedded sandstone (lithofacies Sl). (H) Sandstone with erosional scour and fill (lithofacies Se), with floating carbonate nodules as the lag deposits. (I) Bioturbated sandstone (lithofacies Sb). (J) Convoluted sandstone (lithofacies Sc). (K) Mudstones and siltstones (lithofacies Fs). (L) Laminated siltstones (lithofacies Fl). Legends for lithofacies in logs are shown below the figure panels.

Table 1. Description and interpretation of lithofacies in the McCullough Peaks stratigraphy.

Lithofacies code	Description	Interpretation
Clast-supported conglomerate (**G**)	Poorly sorted, granule to small pebble conglomerate, with medium-grained angular sandstones as the matrix. The conglomerate fills erosional scours and can also be organized into 20 to 60 cm thick beds at the base of sandstone bodies	Intrabasinal clasts of floodplain mudstones or granules deposited by subcritical to supercritical traction flow
Massive sandstone (**Sm**)	Fine to medium-grained sandstone, well-sorted, no apparent sedimentary structures, a few decimetres in thickness	High rate of deposition, probably formed during high-discharge periods
Trough cross-stratified sandstone (**St**)	Fine to coarse-grained, well-rounded sandstone forming up to 50 cm thick cross-stratified beds. Preserved set thickness varying between 5 cm and 30 cm, often decreasing upward in the bed. Sets in the basal part of a sandstone body are often poorly sorted and may contain granules; sets in the top of a bed are better sorted. Claystone chips are common. Bed boundaries are slightly inclined (up to 2 degrees)	Subcritical flow, normal deposition rates, bedload deposition, dune migration
Planar/tabular cross-stratified sandstone (**Sp**)	Fine to medium-grained, well-rounded, and moderate to well-sorted lithic sandstone forming up to 30 cm thick cross-stratified beds. Preserved set thickness varying between 5 cm and 20 cm, often decreasing upward in the bed. Bed boundaries are slightly inclined	Subcritical flow, normal deposition rates, bedload deposition, plane bed formation
Ripple cross-laminated sandstone (**Sr**)	Very fine to fine-grained sandstone, well-sorted, ripple lamination with a set thickness of 2 to 5 cm	Ripple migration under the low-flow regime
Climbing-ripple cross-laminated sandstone (**Scr**)	Fine-grained sandstone, moderately to well-sorted, asymmetrical cross-lamination with climbing set boundaries, with a bed set thickness of 2 to 5 cm	Subcritical flow, faster deposition than ripple migration due to abundant sediments in suspension
Low-angle (<15°) cross-bedded sandstone (**Sl**)	Fine to medium-grained sandstones, well-rounded, moderately to well-sorted, bed thickness of 0.1 to 1.0 m. Low-angle stratification with a long wavelength and low angle	Deposition under upper-flow-regime conditions during high-stage flooding events in nearby channels; or formed as part of a bar clinoform
Sandstone with erosional scour and fill (**Se**)	Fine to medium-grained poorly sorted sandstones, with sand-supported nodules (0.5 to 2.0 cm in diameter) filling the scours, thickness of 0.2 to 1.0 m	Supercritical flow causing the scour, high deposition rates, with nodules as lag deposits
Bioturbated sandstone (**Sb**)	Fine to medium-grained sandstone, moderately to poorly sorted, with vertical and horizontal burrows and trace fossils	Trace fossils formed by insects, dwelling, resting, crawling
Convoluted sandstone (**Sc**)	Fine to medium-grained, well-rounded, moderately to well-sorted lithic sandstone. Preserved set thickness varying between 5 cm and 20 cm, often decreasing upward in the bed. Overturned-fold-shaped structures that modified or destroyed primary sedimentary structures, with a size of 20 to 60 cm	Water escape structures formed in rapidly deposited, poorly sorted sands
Mudstones and siltstones (**Fs**)	Clay to siltstone, with laminated or blocky structures, various matrix colours, common slickensides and nodules	Soil formation with chemical precipitation developed on former overbank fines
Laminated siltstones (**Fl**)	Well-sorted siltstones with ripple laminations	Settling from suspension and forming silty plug in the abandoned channel

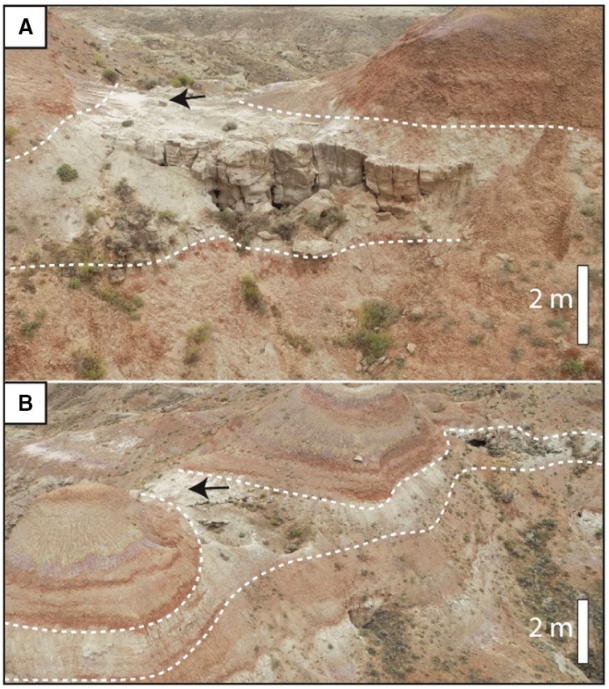

Fig. 4. Facies Association 1: Small-scale crevasse channel sandstone deposit. (A) Unmanned aerial vehicle (UAV) photograph showing the channel body in transverse view. (B) UAV photograph showing the ribbon shape of the same channel body in longitudinal view. The two black arrows in subfigures (A) and (B) point at the same gravel rock debris on the ground.

deposits generally present channelized features with clear gradually-thinning channel wings (Fig. 5A). There is usually an erosional channel base with scouring characteristics, above which trough cross-stratified sandstone (St), planar/tabular cross-stratified sandstone (Sp) and ripple cross-laminated sandstone (Sr) dominate, with occasionally seen convoluted sandstone (Sc; Fig. 5B and C). At some locations, FA2 manifests itself as massive-weathering sandstone bodies that barely have any internal erosional surfaces but have sharp channel margins (Fig. 5D). FA2 is relatively rare (five out of 92 documented channel sandstone bodies) in the study area. Although not always, it mostly (three out of five cases) occurs at the same stratigraphic level as the sinuous-like channel sandstone deposits (FA4), which will be described below.

Interpretation: FA2 is interpreted to have formed in the main threads of the drainage system under the high sedimentation rate conditions. Large sandstone body thickness (>8 m), steep channel margin (for example, Fig. 5E), and the erosional base of the sandstone body indicate deep and strong scouring. Nonetheless, its origin and planform style are not well-understood yet due to the scarcity of FA2 in the study area and limited exposure quality, and more data are needed.

Facies Association 3: Braided-like channel sandstone deposits

Description: Facies Association 3 (FA3) is generally composed of medium-grained sandstones, with conglomerate (G) occasionally seen at the base as lag deposits (Fig. 6). It is usually multi-storied, and sharp erosional bases are present between storeys. Within a single storey, sandstone with erosional scour and fill (Se) and trough cross-stratified sandstone (St) are present in the lower part, planar/tabular cross-stratified sandstone (Sp) is in the middle part, and ripple cross-laminated sandstone (Sr) and low-angle (<15°) cross-stratified sandstone (Sl) are in the upper part, occasionally replaced by massive sandstone (Sm; Fig. 6D). The dip direction of the accretion surfaces is generally parallel to measured palaeocurrent directions in cross-bedded sets.

Forty-eight FA3 sandstone bodies are documented in this study, with a thickness range of 4 to 8 m, an average thickness of 6.1 m, and a standard deviation of 2.4 m (Fig. 7A). Their apparent widths as measured in the photogrammetric model were corrected using the average palaeoflow direction (N 004°; Fig. S1; Fabuel-Perez *et al.*, 2009), yielding an average of 203 m and a standard deviation of 137 m (Fig. 7B). These braided channel sandstone bodies commonly have three to four storeys, with a thickness range of 0.5 to 2.0 m and an average storey thickness of 1.7 m ($n = 151$). The sandstone body aspect ratio, defined as the width/thickness ratio, has an average of 38 and a standard deviation of 28 (Fig. 7C). Dune-scale cross-sets in FA3 ($n = 45$) have an average preserved thickness of 22 cm, with a standard deviation of 13 cm and a coefficient of variation (CV) of 0.59 (Fig. 7D). Using these dune-set data and employing existing empirical relationships (e.g. Bridge & Tye, 2000; Leclair & Bridge, 2001), the average bankfull depth is estimated to be 4.3 m (22 cm × 2.9 × 6.7). The high CV (0.59) ensures the reliability of the estimation of the formative flow depth using cross-set thickness (Bridge & Tye, 2000).

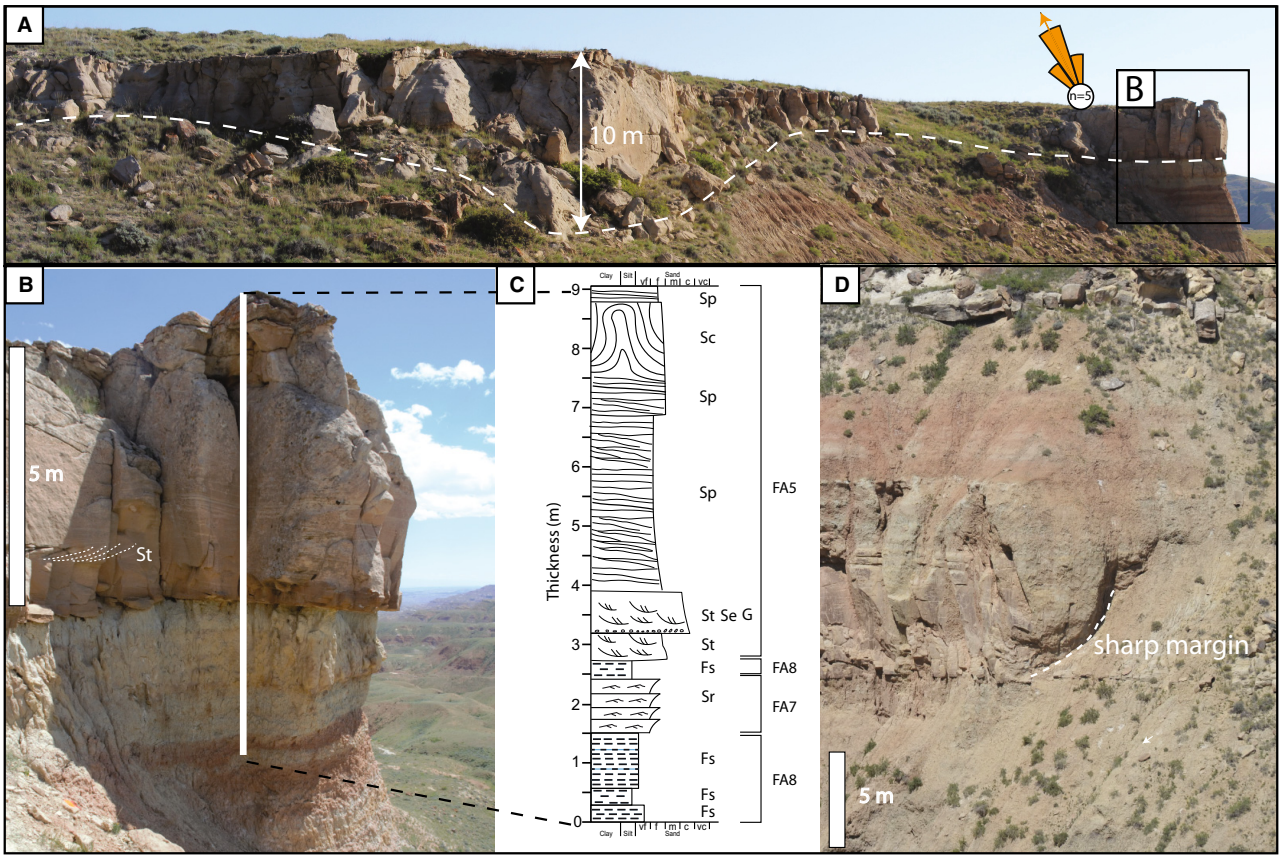

Fig. 5. Facies Association 2: Large-scale trunk channel sandstone deposit. (A) Overview of the large-scale trunk channel sandstone deposits with a maximum thickness of *ca* 10 m. (B) and (C) Zoomed-in view and log of the right side of subfigure (A) showing detailed sedimentary structures and underlying floodplain fines. The white line marks the corresponding sedimentological log position. (D) A second example of FA2 deposits that have a maximum thickness of *ca* 10 m with sharp channel margins eroding into floodplain fines and a thin splay bed in the lower part. For legend, see Fig. 3.

Planar/tabular cross-stratified sandstone (Sp) and low-angle (<15°) cross-stratified sandstone (Sl) are dominant lithofacies in FA3, accounting for 51% and 15%, respectively (Fig. 7E). Palaeoflow rose diagrams show a mean flow direction of N 016° and a standard deviation of 90° (Fig. 7F). The distribution of the palaeoflow data is significantly different from the uniform distribution according to the Rayleigh test of uniformity (0.29 with a *P*-value of 0).

Microscopic observation of 28 thin sections shows that monocrystalline quartz grains in FA3 are generally subrounded to subangular and slightly spherical (Fig. S2A and B), and they are classified together with polycrystalline quartz (quartzite) and microcrystalline quartz (chert) as 'quartz' in the scheme developed by McBride (1963). Feldspar content varies widely, with potassium feldspar (for example, orthoclase and microcline) more dominant than plagioclase (for example, albite). Rock fragments include sedimentary, volcanic and metamorphic components. Accessory (heavy) minerals are either of igneous or metamorphic origin, and include magnetite, zircon, tourmaline and hornblende. Both calcite and silica cement are observed, with the former contributing to the mosaic granular framework and the latter causing euhedral to subhedral quartz/feldspar overgrowths.

Interpretation: FA3 presents characteristics normally ascribed to the sedimentary product of braided river processes. This interpretation is supported by the predominance of medium to coarse-grained bedload material, the scarcity of lateral accretion deposits, the abundance of downstream accretion deposits, no fining upward grain-size profile, little or no fine-grained sediment and/or soil preservation, and the stacking of several single-storey units within individual

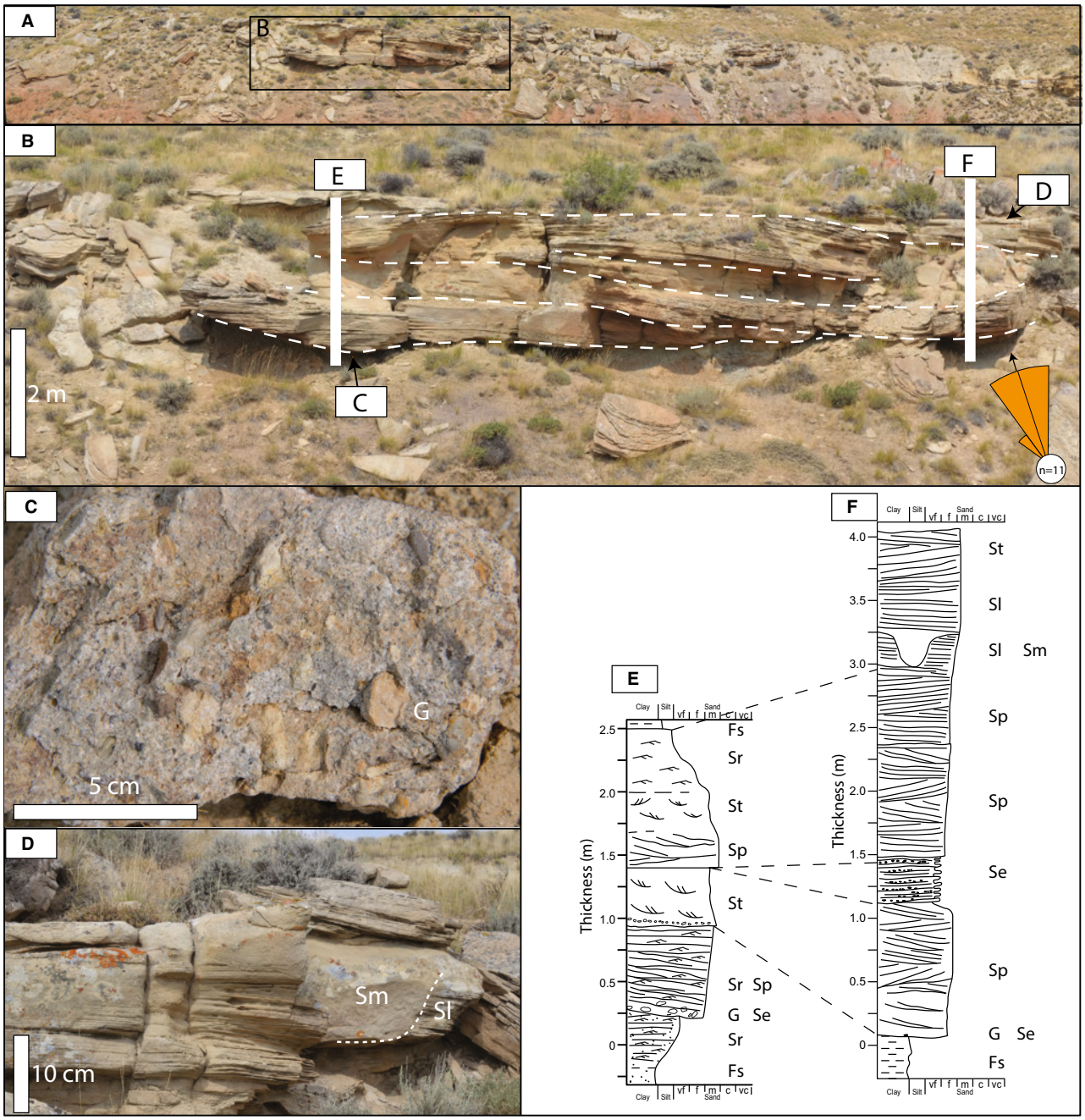

Fig. 6. Facies Association 3: Braided-like channel sandstone deposits. (A) and (B) Overview and close-up view of FA3 deposits, where there are five storeys with the thickness of each varying between 0.5 m and 1.0 m. (C) The bottom view of the channel base with floodplain nodules as lag deposits. (D) Massive bank-breaching deposits (Sm; *cf.* van den Berg *et al.*, 2017) eroding low-angle cross-bedded sandstone (Sl). (E) and (F) Sedimentary logs for locations in panel (B), showing the vertical succession of lithofacies in FA3. For legend, see Fig. 3.

sandstone bodies (Leopold & Wolman, 1957; Bridge *et al.*, 1986; Gibling, 2006; Sambrook Smith *et al.*, 2006; Foreman, 2014; Hartley *et al.*, 2015, 2018; Limaye, 2020). The presence of some fine-grained deposits below erosional surfaces suggests channel abandonment and reoccupation. Single-storey units in FA3 are generally narrow and thin, indicating their short life spans and quick lateral coalescence of multiple channel storeys (Gibling, 2006). In general, braided

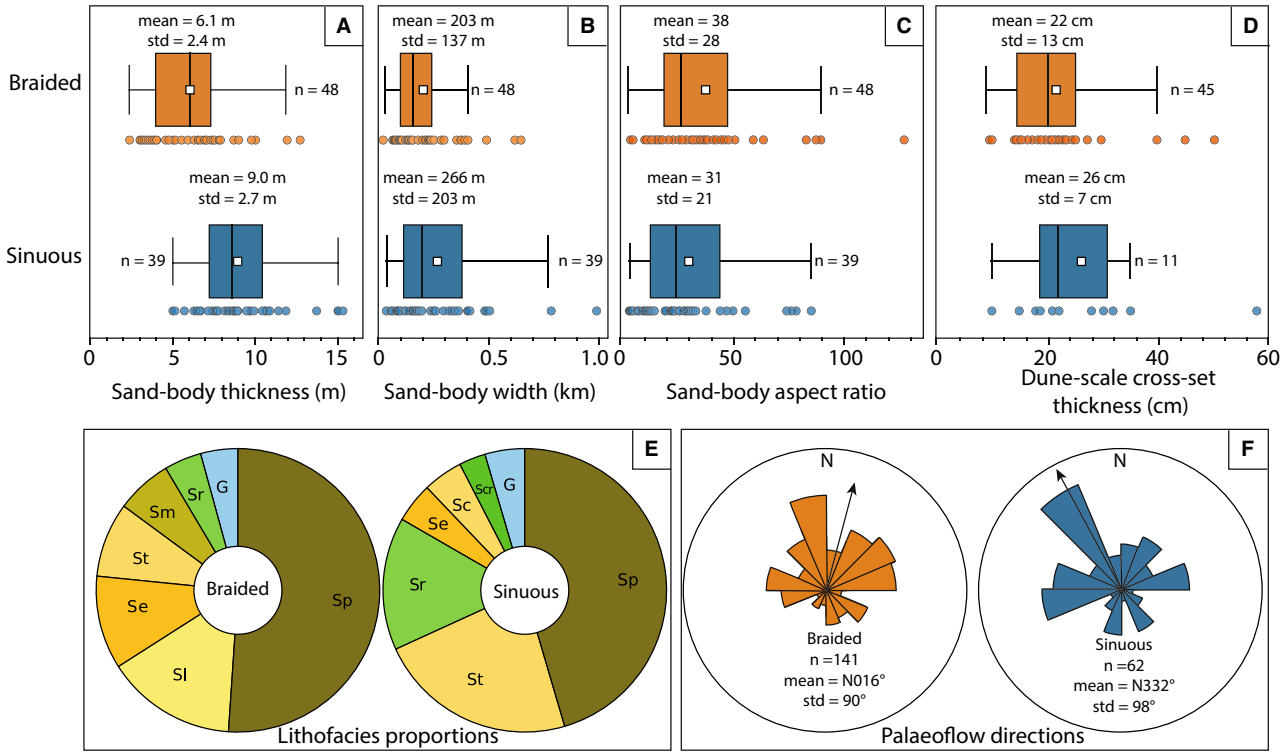

Fig. 7. (A) Thicknesses, (B) widths and (C) aspects of braided-like and sinuous-like channel sandstone bodies. (D) Thicknesses of dune-scale cross-sets. (E) Relative abundance of different lithofacies within braided-like and sinuous-like channel sandstone bodies (abbreviations are listed in Table 1). (F) Rose diagrams of palaeoflow directions. Note the significantly thinner and insignificantly narrower braided-like channel sandstone bodies than sinuous-like counterparts, the similarity and difference between relative lithofacies abundance, and the similarity and difference between palaeoflow directions.

channels tend to occur in a range of environments associated with rapid and frequent variations in water discharge, high sediment load, coarse sediment grain size, high gradient and erodible banks (Leopold & Wolman, 1957; Schumm, 1985; Summerfield, 1991; Bridge, 1993; Church, 2006; Ashmore, 2013; Limaye, 2020).

Facies Association 4 — Sinuous-like channel sandstone deposits

Description: Facies Association 4 (FA4) is generally composed of: (i) poorly-sorted, subangular, coarse-grained trough cross-stratified sandstones (St) with granules (G) and sandstones with erosional scour and fill (Se) at the base; (ii) large-scale inclined strata with moderate to well-sorted medium-grained trough cross-stratified sandstones (St) and planar cross-stratified sandstones (Sp) in the middle; and (iii) fine-grained ripple-laminated sandstones (Sr) at the top (Fig. 8). The basal part is usually 0.5 to 1.0 m thick, while the middle and upper parts are generally >4 m thick. Both dune-scale cross-stratification (Fig. 8D) and ripple-scale cross-lamination sedimentary structures are present. Accretion beds (Fig. 8B) are inclined approximately perpendicular to or at a large angle with measured palaeocurrent directions from cross-stratified bedforms. Water-escape structures are occasionally seen in convolute sandstone (Sc) within lateral accreted deposits (Fig. 8C).

A set of four well-preserved point bars constitutes a series of bends along a downstream-oriented sinuous channel belt in the map view, as corroborated by the laterally traceable palaeosol layer over approximately 2.0 km on top of these point bars (Fig. S1H). Lateral accretion surfaces of these point bars all dip in the same direction at a large angle with the measured palaeocurrent directions from cross-stratified bedforms. Individual point bars of this set are 0.2 to 0.5 km wide, 0.1 to 1.2 km long and 7.0 to 11.0 m thick, presenting features both parallel and perpendicular to the palaeoflow direction.

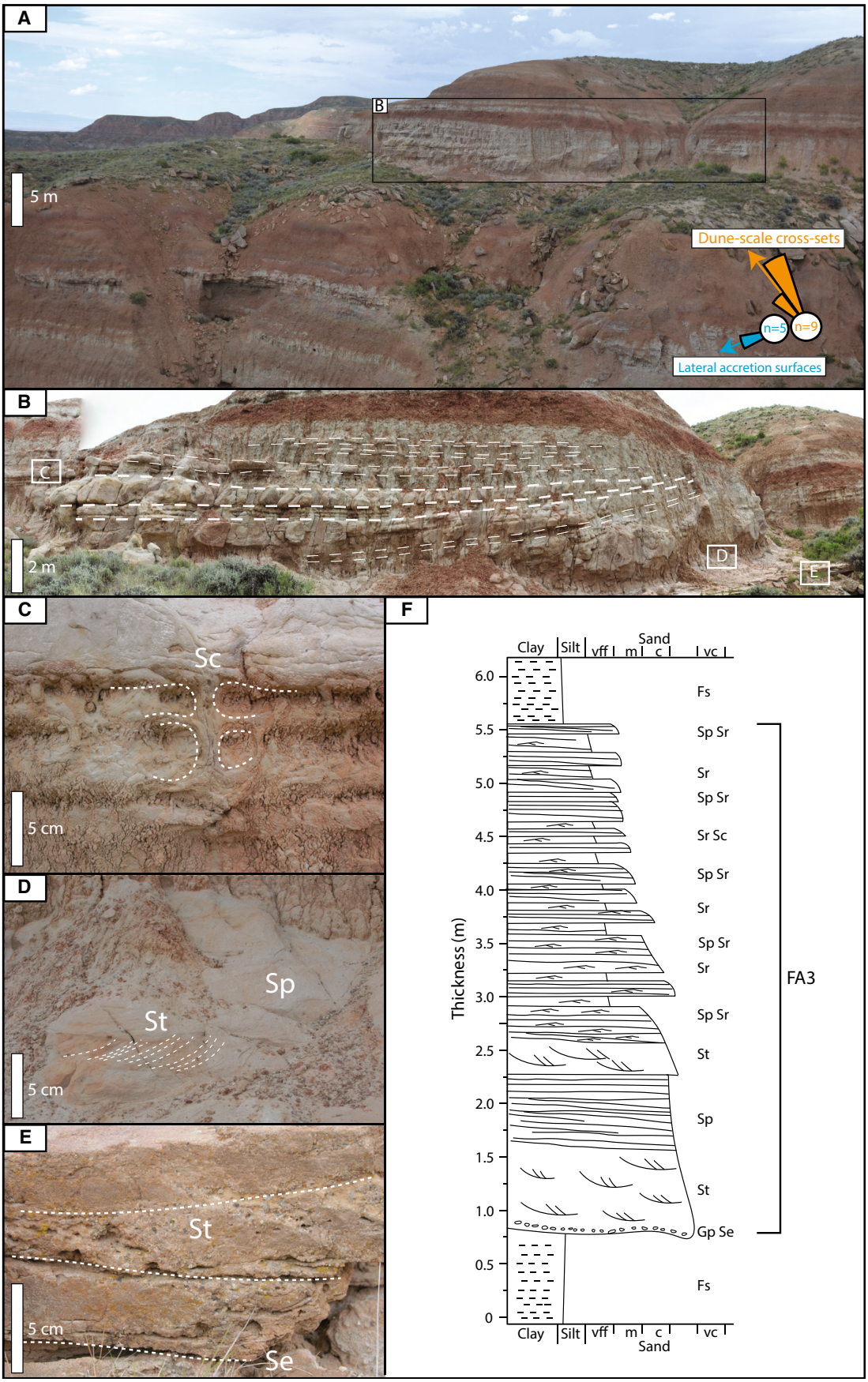

Fig. 8. Facies Association 4: Sinuous-like channel sandstone deposits. (A) Overview photograph showing the juxtaposition between FA4 and surrounding strata. (B) Enlarged view of the FA4 deposits, where lateral accretion deposits are distinct, as indicated by dashed lines. Letters 'C' to 'E' in the white boxes marked on this subfigure indicate the positions of subfigures (C) to (E). (C) Convolute sandstone with clear water escape structures. (D) Trough and planar cross-bedding with a dominant flow direction of 10°. (E) Channel-floor deposits at the base of FA4. (F) Composite sedimentary log illustrating the vertical succession of lithofacies in FA4. For legend, see Fig. 3.

The map view of these point bars using their 3D coordinates from the photogrammetric model makes it possible to calculate the channel sinuosity index (Fig. S1H), which is 1.8 and thus falls into the category of meandering river planform (Williams, 1986).

Thirty-nine sandstone bodies with FA3 are documented. The average thickness is 9.0 m while the standard deviation is 2.7 m (Fig. 7A). Apparent field measurements of these sandbodies are corrected against the average palaeoflow direction (N 004°; Fig. S1), yielding an average value of 266 m and a standard deviation of 203 m (Fig. 7B). The sandstone body aspect ratio has an average of 31 and a standard deviation of 21 (Fig. 7C). Preserved dune-scale cross-sets in FA4 ($n = 11$) have an average thickness of 26 cm with a standard deviation of 7 cm and thus a coefficient of variation (CV) of 0.29 (Fig. 7D). From these data and the application of existing empirical relationships (Bridge & Tye, 2000; Leclair & Bridge, 2001), the average bankfull depth is calculated to be 5.1 m (26 cm × 2.9 × 6.7), which is consistent with the thickness of the inclined strata (commonly >4.0 m). The low CV (0.29, required to range between 0.58 to 1.18) renders it uncertain to estimate the formative flow depth using preserved cross-set thickness (Bridge & Tye, 2000). Planar/tabular cross-stratified sandstone (Sp) and trough cross-stratified sandstone (St) are predominant lithofacies in terms of the lithofacies proportions in thickness, accounting for 45% and 23%, respectively (Fig. 7E). The palaeoflow measurements ($n = 63$) present a mean flow direction of N 332°, with a standard deviation of 98° (Fig. 7F). The distribution of the palaeoflow data in FA4 is significantly different from the uniform distribution according to the Rayleigh test of uniformity (0.23 with a *P*-value of 0.04).

Compared with FA3 braided-like channel sandstone bodies, sinuous-like counterparts are significantly thicker ($t = 5.3$, $P = 0.9 \times 10^{-7}$) and insignificantly wider ($t = 1.4$, $P = 0.16$) according to the *t*-test. However, dune-scale cross-sets in FA4 sinuous-like channel deposits are not significantly different from those in FA3 braided-like channel deposits ($t = 0.6$, $P = 0.5$), although the average preserved thickness of the former is higher than that of the latter. In terms of palaeoflow measurements, there is no significant difference between braided-like and sinuous-like channel deposits at a 0.05 level of significance according to Watson's Two-Sample Test of Homogeneity, which is likely attributable to the large standard deviations of both measurements (90° and 98°, respectively).

There are three available thin sections for FA4 sandstone bodies. Compared with FA3, FA4 is overall finer and has higher abundances of quartz and chert (Fig. S2 C and D).

Interpretation: FA4 presents the characteristics that are normally ascribed to sinuous river processes. Accretion beds are aligned broadly perpendicular to the overall palaeoflow direction, and they are inferred as lateral accretion beds (Fig. 8B). These lateral accreted deposits result from the reduced shear stress associated with helicoidal flows, which leads to erosion in the outer bend and lateral migration of the point bar located in the inner bend in the same direction (Bridge, 1993). The lower coarser-grained segment of the sandstone bodies represents the channel lag interval. In general, sinuous channels tend to occur in a range of environments associated with perennial flow, relatively low sediment load, low gradient and cohesive overbank materials (Leopold & Wolman, 1957; Schumm, 1985; Church, 2006). Nevertheless, recent progress in understanding high-sinuosity rivers has been contesting these generic models. For instance, many more sandy sinuous systems have been documented in the laboratory and depositional basins (e.g. Braudrick *et al.*, 2009; Hartley *et al.*, 2015, 2018), which indicate that the low sediment load is not necessarily a prerequisite for sinuous river channel development. Therefore, no single factor can be determined to definitively contribute to sinuous river channel development, and a combination of several factors should be implemented for higher-certainty interpretation.

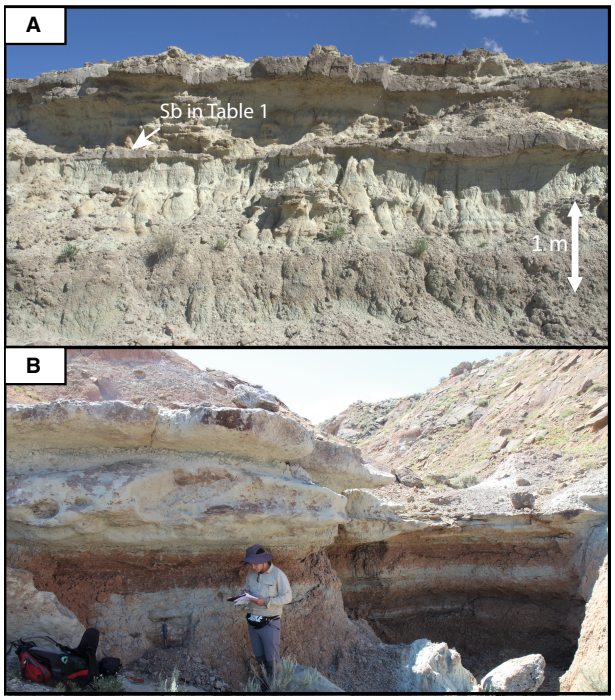

Fig. 9. Facies Association 5: Sheet-like crevasse splay deposit. The person for scale in panel (B) is *ca* 1.8 m.

Floodplain facies associations

The floodplain deposits have been described extensively in numerous studies (e.g. Kraus, 1987; Kraus & Bown, 1993; Kraus & Gwinn, 1997; Kraus & Hasiotis, 2006; Abdul Aziz *et al.*, 2008; Abels *et al.*, 2013; Wang *et al.*, 2021). Here, only the sandy floodplain facies association is documented.

Facies Association 5 Sheet-like crevasse splay deposits

Description: Facies Association 5 (FA5) consists of very fine to coarse-grained sandstones (Fig. 9A). It is in many cases composed of multiple beds, with the thickness of an individual bed ranging from 0.1 m to 0.5 m. FA5 sediments are in general well-sorted. Trough cross-stratified sandstone (St), low-angle (<15°) cross-stratified sandstone (Sl) and ripple cross-laminated sandstone (Sr) are the most dominant lithofacies, typically presenting upward coarsening trends. The lateral extent of FA5 can be up to a few kilometres as measured from the photogrammetric model and traced in the field, which depends on the direction in which it is measured. Burrows are observed to be oriented in random directions (Facies Sb in Fig. 3). The palaeocurrents measured in FA5 deposits are generally oblique to the main channel from which the deposit originates. FA5 deposits are prevalent throughout the entire stratigraphy, forming the 'heterolithic' deposits of Abels *et al.* (2013).

Interpretation: FA5 is interpreted to represent unconfined flow conditions on the floodplain, as part of a splay complex formed during erosion of the channel levée (Davies-Vollum & Kraus, 2001; Fisher *et al.*, 2007). Multiple beds may represent multiple events of crevasse processes. FA5 has been commonly referred to as heterolithic deposits produced by crevasse splaying and overbank flooding processes (e.g. Kraus & Aslan, 1993; Kraus & Wells, 1999; Abels *et al.*, 2013; Foreman, 2014).

Spatial distribution of channel sandstone bodies

The highest point of a channel sandstone body in the 3D photogrammetric model is assigned as the representative point for this sandstone body. Thus, it becomes feasible to project the locations of all of the channel sandstone bodies in the 3D space, including five large-scale trunk channel sandstone bodies (FA2), 48 braided-like channel sandstone bodies (FA3) and 39 sinuous-like channel sandstone bodies (FA4). Crevasse channel sandstone bodies (FA1) are not projected because they cannot be always confidently recognized in the field when direct access is unavailable nor in the photogrammetric model because of their relatively low thickness. Large-scale trunk channel sandstone deposits (FA2) are relatively rare (five out of 92) and thus will not be analysed in detail below. Therefore, the main focus will be on FA3 and FA4, even though it may be possible that the FA2 systems may have played a relatively large role at the basinal scale.

From the horizontal XY plane of Fig. 10, it can be seen that FA3 and FA4 occur in an intercalated fashion. In other words, laterally (along the XY horizontal plane), FA3 or FA4 are not confined to certain portions of the study area, and appear randomly distributed. Projection of the channel sandstone bodies from 3D space onto the YZ plane shows a pseudo-downstream-oriented stratigraphic profile, but it is not done here because it requires adjustments to tectonic tilt, faults and integration with floodplain stratigraphy. This will be done systematically in a future study.

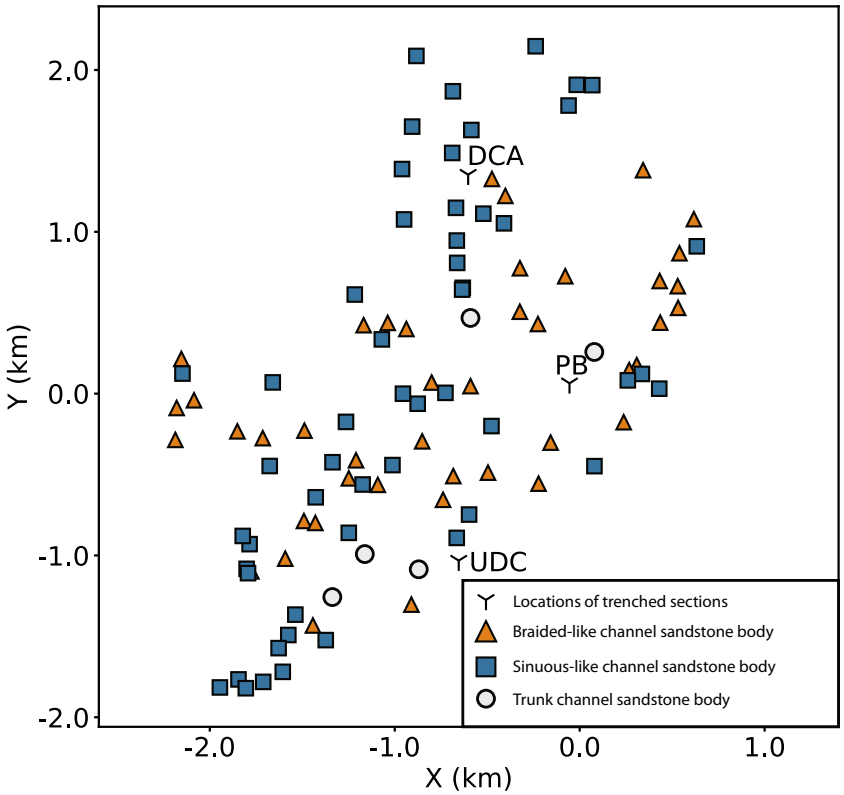

Fig. 10. Projection of sandstone bodies from 3D space to 2D XY horizontal plane. X and Y coordinates are converted from global UTM coordinates (zone 12N) to local ones, with an applied offset of (673 000 m, 49 242 600 m). Abbreviations: DCA, Deer Creek Amphitheatre section (Abels *et al.*, 2013); UDC, Upper Deer Creek section (Abels *et al.*, 2012); CSH, Creek Star Hill section (Abels *et al.*, 2016); and PB, Purple Butte section. Locations of these trenched sections can be found in Fig. 2.

DISCUSSION

River planform identification

Results from the integrated field analysis allow for a discussion on the difference in flow conditions associated with sandstone bodies of different river styles. As mentioned in the *Spatial distribution of channel sandstone bodies* section, the main focus of this study is on FA3 ($n = 48$) and FA4 ($n = 39$) channel sandstone bodies, features of which point to braided-like and sinuous-like river planform styles, respectively. Nonetheless, the above interpretation of river styles is inevitably influenced by the limitations of available outcrop and our inherent inability to distinguish river planform morphology from near-vertical outcrop sections. Lithofacies and their associations are the most direct and helpful indicators of river planform morphology, but they are not necessarily definitive. In other words, the braided-like and sinuous-like morphology can be caused by different factors that result in a similar end product.

Lateral accretion sets are regarded as the key to the distinctive separation of braided and sinuous systems (Davies & Gibling, 2010; Hartley *et al.*, 2018), but their absence in the outcrop sections does not always imply a braided planform style, which brings uncertainties in identifying braided channel deposits. Holbrook & Allen (2021) report a case of a braided river that meanders, which means the above interpretations may be biased if only parts of the outcrop are observed. Moreover, since braided and sinuous rivers constitute a continuum in river planform styles, the study area may also be possibly situated in a transitional zone between sinuous and braided-river-dominated zones, and thus the two main interpreted river planform styles may not be too far from one another. What is documented in this study, therefore, may not be the absolute end members (i.e. sinuous and braided river planforms), and instead there may be mixed systems in the basin. A detailed stratigraphic analysis is needed to elucidate the stratigraphic occurrence of the two seeming end-members recognized in this study. Initial observations suggest occasional close stratigraphic proximity of FA3 and FA4 sandbodies, while intervals dominated by one of these two Facies Associations also seem to occur.

Another important issue in our interpretation is the potential over-reliance on the river planform attribution. For instance, the low-angle cross-bedded sandstone (Facies Sl) recognized

in the FA3 braided-like channel deposits is inferred above to be formed in the upper flow regimes (Lorenz & Nadon, 2002; Fielding, 2006), and an increase in the upper flow regime structures is suggestive of braided river morphology. However, Facies Sl could also be a part of the bar clinoform that does not require upper flow conditions (Ethridge & Schumm, 1978; Foreman *et al.*, 2012). Moreover, as noted by many researchers (e.g. Davies & Gibling, 2010; Gibling & Davies, 2012; Santos *et al.*, 2016; Hartley *et al.*, 2018), it is notoriously difficult to distinguish between braided and sinuous river planforms if the deposits are coarse-grained, because they may have very similar characteristics. In this context, it might be more conservative and objective to attribute FA3 and FA4 to two scenarios of fluvial deposition: one that is more perennial or uniform in discharge and one that is more ephemeral or peaked in discharge (Plink-Björklund, 2015; Fielding *et al.*, 2018). This interpretation would pertain to our dataset but avoid invoking whole-scale changes in planform morphology, given the fact that the braided-like and sinuous-like channel sandstone bodies are not significantly different from one another in terms of width, aspect ratio and palaeoflow direction, although they do differ significantly from one another in relation to the thickness (Fig. 7).

Disregarding the fully acknowledged difficulties in attributing these fluvial deposits to two end-member river planforms, the authors further refer to FA3 as braided-like and FA4 as sinuous-like river styles for the simplicity of the below general discussion while still referring to the fact that these are not strictly the end-members of a continuum of river planform styles.

Bighorn Basin river styles and flow conditions

As discussed above, all of the interpreted river styles are based on the best knowledge of the authors on the available outcrop data. Owing to the dominant abundance and geological importance, FA3 and FA4 deposits are the main focus of discussion, while acknowledging that FA2 needs further study.

FA3 braided-like channel sandstone deposits and FA4 sinuous-like channel sandstone deposits present both similarities and differences. First of all, the most dominant lithofacies in both of these deposits is the planar cross-stratified sandstone (Sp; Fig. 7E), which is the result of straight-crested bedforms in the lower flow regime with intermittent to continuous sand motion and subcritical water flow conditions (Harms & Fahnestock, 1965; Coleman, 1969; Bourquin *et al.*, 2009; Went & McMahon, 2018). The second most dominant lithofacies in FA3 braided-like channel sandstone deposits is low-angle (<15°) cross-bedded sandstone (Sl), which is formed in upper flow regimes, accompanied by high sediment concentration and continuous sand motion (Harms & Fahnestock, 1965; Coleman, 1969; Bourquin *et al.*, 2009; Went & McMahon, 2018). In contrast, the second most dominant lithofacies in FA4 sinuous-like channel sandstone deposits is trough cross-stratified sandstone (St), which is the result of linguoid bedforms that mainly develop in the subcritical lower flow regimes. Based on the two most dominant lithofacies in FA3 and FA4, the flow velocity that produces FA3 braided-like channel sandstone deposits is in general higher than that which produces FA4 sinuous-like channel sandstone deposits. From the perspective of Froude number calculation (Kennedy, 1969), FA3 braided-like channel sandstone deposits should be formed in a condition of either higher velocity or shallower water depth or a combination of both than FA4 counterparts.

The narrow and thin single-storey units in FA3 indicate short life spans and quick lateral coalescence of multiple channel storeys that may result from multiple phases of ephemeral flow (Gibling, 2006) or spike-like discharge conditions (Fielding *et al.*, 2018). In contrast, the presence of lateral accretional surfaces and the sinuosity index up to 1.8 (Figs 8 and S2H) in FA4 suggest more stable, perennial water flow conditions. More importantly, FA3 braided-like channel deposits are significantly thinner and insignificantly narrower than FA4 sinuous-like channel deposits, which indicates that FA3 may be formed in flashy-discharge conditions instead of continuously high-discharge conditions (Fielding *et al.*, 2018).

The insignificant difference in palaeoflow directions between FA3 and FA4 suggests that they may have developed in channel belts with similar downstream orientation. Measurements of palaeoflow directions in FA4 sinuous-like channel sandstone deposits are not uniform, and this is expected because they vary with the locations with reference to the meander bend and should show a large spread when plotted altogether. Meanwhile, those in FA3 braided-like

channel sandstone deposits are also different from the uniform distribution, and they have a large circular deviation (standard deviation = 90°) and present a dispersal pattern similar to the FA4 sinuous-like channel sandstone deposits (standard deviation = 98°). Pryor (1960) suggested that the slope of the depositional surface is the most important factor controlling the circular deviation and dispersal pattern of the palaeoflow data, with a larger slope contributing to more uniform palaeoflow data. Therefore, it can be inferred that the slope was gentle for both FA3 and FA4 deposition. In this context, discharge difference might be the main contributor to the river planform style change (Leopold & Wolman, 1957). Nevertheless, a wide range of palaeocurrents is also expected in braided rivers when there is local flow deflection around bars (Miall, 1994). Therefore, the hypothesis of slope gentleness needs more analysis before argumentation. Moreover, it is worthwhile to highlight that palaeocurrent dispersal alone cannot be used as a criterion to distinguish sinuous and braided channel deposits (Ghinassi & Ielpi, 2015; Ghinassi *et al.*, 2016; Hartley *et al.*, 2018).

Geomorphic zonation of the Bighorn Basin

Literature shows that braided rivers evolve into sinuous rivers when certain thresholds in water and sediment discharge and/or slope are exceeded (Leopold & Wolman, 1957; Bridge, 2003). As analysed in the above section, the study area might represent a gentle slope during the deposition of FA3 and FA4, and thus the discharge condition may play a critical role in determining the river planform styles. The study area is far from the southern Owl Creek Mountains and, if that is the only catchment, sinuous rivers should develop in the study area according to the geomorphic zonation theory in river basins (Schumm, 1985). However, braided-like channel deposits do occur in many cases (48 FA3 versus 39 FA4) in the study area. Existing data suggest that there might have been multiple feeding systems influencing the study area from the western catchments (Kraus, 1980; Wing & Bown, 1985; Owen *et al.*, 2019). Given the proximity of the study area to the western catchment and the high gradient from the western basin margin relative to the southern and eastern margins in the early Eocene, the study area will likely have been fed by multiple western systems that confluence with an axial system flowing from south to north, as has been demonstrated in Owen *et al.* (2019). Similar depositional models that include transverse and axial river systems have been reported in modern and ancient outcrop analogues as well as flume experiments (e.g. DeCelles *et al.*, 1991; DeCelles & Cavazza, 1999; Weissmann *et al.*, 2015; Giles *et al.*, 2016; Kim *et al.*, 2011; Connell *et al.*, 2012).

The southern and eastern catchments are thought to have been lower and possibly more dominated by the reworking of Mesozoic fines (DeCelles *et al.*, 1991). With the feeding of basement-rich western source materials into the axial system of the basin, the sinuous systems may have been alternated or changed into braided systems downstream where discharge was temporarily increased. Quantitative basinal data are provided in Owen *et al.* (2019), where a wide axial fluvial system is identified that characterizes reverse downstream distributive fluvial system trends (i.e. decreasing channel portion and dimension as well as grain size) and they ascribe this to influences of transverse systems of variable size at different sites with respect to the axial system. The present study could be in line with the interfingering between an axial system and possibly the Absoraka or Washakie transverse systems in terms of sediment and discharge, while the study site is probably too far downstream to see the direct interfingering site of these systems, as suggested by our and basin-wide palaeocurrent data.

The Washakie Range, which is now partly covered by the Absaroka Mountains (Fig. 2), was present during the deposition of the Willwood Formation, and is hypothesized to have been an important catchment for the transverse system (Owen *et al.*, 2019). This suggestion is supported by the presence of fanglomerates of Palaeocene age in the western margin of the basin (Kraus, 1984). There could also have been an 'Absaroka' transverse system in the north of the Washakie system (van Houten, 1944; Sundell, 1990), which is more proximal to our study area and could have played a more important role as a transverse system directly feeding the study area.

The study area is relatively small compared with the basin size, and thus data from published studies are needed to provide information at other sites of the basin. Willwood sheet sandstones documented very close to our study area (*cf.* Friend, 1983; Kraus & Middleton, 1987) are believed to be generated by laterally mobile or meandering streams in the major axial system,

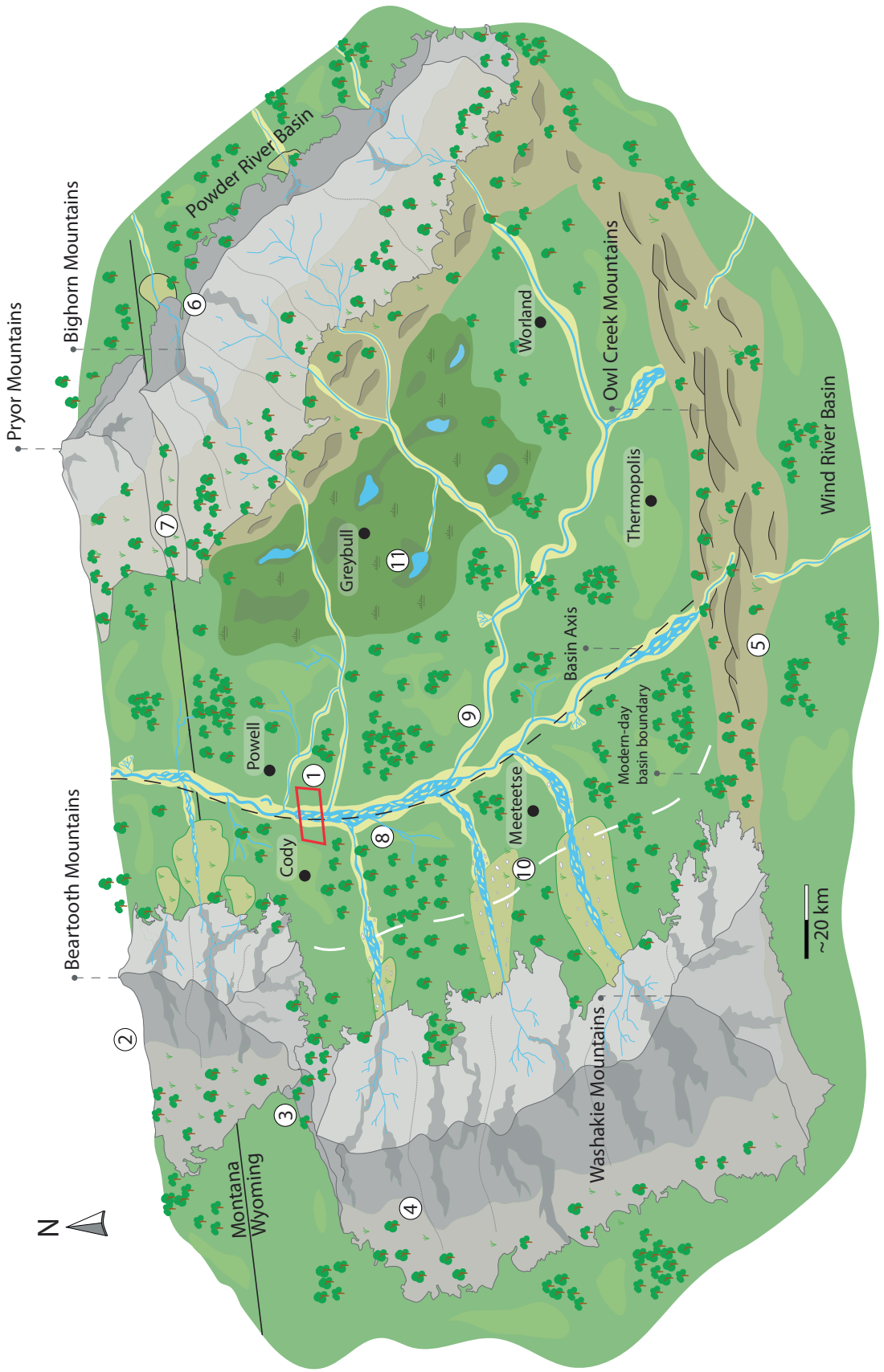

Fig. 11. Schematized palaeogeographical model of the Bighorn Basin during the early Eocene. Avulsion is a prevailing behaviour of the Willwood system but it is only sporadically portrayed here so as not to obscure the river planform style alternation. Annotations for elements marked with numbers in the figure are as follows: (1) The McCullough Peaks study area. (2) The Beartooth Mountains with a very steep eastern flank (Bown, 1980) and several ephemeral coarse-grained alluvial fans and braid-plain deposits (DeCelles *et al.*, 1991). (3) The space between the Washakie Mountains and the Beartooth Mountains during the Eocene is uncertain in the literature due to the covering of the Absaroka Mountains. (4) Washakie Mountains are not present today (Kraus, 1985), because they are covered by volcanic Absoraka Mountains (Sundell, 1990). Its exact extent is currently unknown, and several hypotheses exist (van Houten, 1944; Kraus, 1985; Sundell, 1990; Lillegraven, 2009; Owen *et al.*, 2019). (5) The Owl Creek Hills were relatively gentle in the Eocene (Wing & Bown, 1985; Hoy & Ridgway, 1997). (6) Unlike the present day, the Bighorn Mountains were much smaller and not fully formed in the Eocene (Hoy & Ridgway, 1997; Yonkee & Weil, 2015). The small fine-grained sediment input from the Bighorn Mountains into the Bighorn Basin is speculated to be present (Kraus & Middleton, 1987), but this is uncertain given the large distance and gentle topography from the mountains to the axis and the absent palaeocurrent records from the east (Owen *et al.*, 2019). (7) Pryor Gap could be an exit for the rivers during the Eocene (Blackstone, 1940). However, there are no constraints on when it opened. (8) Braided channel belt with downstream accretion deposits. (9) Sinuous channel belt with crevasse splay, local/regional avulsion and point bars. (10) Fanglomerates on the alluvial fan (Kraus, 1983, 1984; Malone *et al.*, 2017; Syzdek *et al.*, 2019), indicating a near-source system. (11) Poorly drained floodplain, swampy and/or lacustrine environments in front of the Bighorn Mountains indicated by organic-rich beds and gley palaeosols (Wing & Bown, 1985; Davies-Vollum & Wing, 1998; Davies-Vollum, 1999, 2001).

as corroborated by the presence of lateral accretion surfaces (Kraus & Middleton, 1987), the greatly varied palaeoflow direction in vertically adjacent storeys (Kraus & Middleton, 1987) and sequences of depositional facies in the sheet sandstones (Kraus, 1980). The work by Foreman (2014) suggests that the Palaeocene–Eocene 'boundary sandstone', 2 million years older than the Willwood strata studied here, was meandering in origin in the Sand Coulee area, which is further downstream to the north of our study area. The sedimentological work by Owen *et al.* (2017) suggests the presence of five channel body geometries, including massive (M), semi-amalgamated (SM), internally amalgamated (IA), offset stack (OS) and isolated (I) forms. According to the included lithofacies associations in these geometries, M is dominantly braided, SA is primarily braided while secondarily meandering, IA is primarily meandering while secondarily braided, and OS and I are mostly meandering (Owen *et al.*, 2017). Projections of these channel body geometries onto the basin map suggest the potential presence of transverse systems at the Beartooth Mountains and the intersection between the current Absaroka Mountains and Owl Creek Mountains (see fig. 12 of Owen *et al.*, 2017). The downstream increasing IA proportion and decreasing I and OS proportions, particularly obvious near our study area, suggest the interference of transverse systems with the axial system. In other words, the axial system should be more dominated by the meandering river planform at the northern part of the basin but, instead, the braided river planform is observed to increase due to the input from the transverse system, as evidenced by both the basin-scale study of Owen *et al.* (2017) and the more local study reported here.

Based on the above analyses and existing research, the palaeogeography of the Bighorn Basin during the early Eocene is refined in map view (Fig. 11), which well represents field observations of this study and data from previous studies, particularly the basin-scale depositional model of Owen *et al.* (2019). Detailed annotations of elements in this map are listed in the caption for Fig. 11, with reference to published literature and this study. The presented palaeogeographical model represents one possible scenario where FA3 braided channel deposits are dominant in the study area during periods of high or ephemeral discharge conditions (Fielding *et al.*, 2018). There are other scenarios plausible when the study area hosts FA4 sinuous channel deposits, probably during the low/perennial discharge conditions based on the analysis in the *River planform identification* section.

To briefly summarize, water discharge in the main stream is determined by contributions from both axial and transverse systems at the upstream part of the study area, and high/ephemeral discharge conditions favour FA3 braided-like channel development while low/perennial discharge conditions favour FA4 sinuous-like channel development (*cf.* Fielding *et al.*, 2018).

Controls on river planform styles and geomorphic zonation

River planform styles depend on several controlling conditions, including water discharge, transport material (bedload versus suspended load), sediment concentration, valley gradient and bank material strength (Schumm, 1985; Church, 2006). In an equilibrium-state river channel, sediment concentration is in balance with the valley gradient (Muto *et al.*, 2007; Wang *et al.*, 2021). These controlling conditions are also influenced by upstream factors, and the sediment concentration can at times be greater than the transport capacity determined by valley gradient and stream power. When this happens, aggrading and braiding fluvial conditions tend to occur (Schumm, 1985; Church, 2006; Muto *et al.*, 2007). In contrast, the river will tend to entrain sediment and degrade when sediment concentration is lower than the transport capacity, and the preferred mode of transient degradation for the channel is to become more sinuous until the channel gradient is reduced to the required value (Bettess & White, 1983), unless bank strength prevents it from reaching the equilibrium gradient (Church, 2006). Nevertheless, sinuous systems are also reported in aggrading schemes (e.g. Willis & Tang, 2010; Ghinassi *et al.*, 2014; van de Lageweg *et al.*, 2015), which should be noted in linking the river planform type and depositional setting during the outcrop interpretation. Therefore, the climatically-controlled sediment concentration can lead to river planform style change by shifting the geomorphic zonation boundaries between two adjacent river styles towards upstream or downstream directions (Holbrook *et al.*, 2006). Understanding on what timescale this process is occurring needs more study. Climate changes, possibly related to astronomical forcing, may have been a dominant contributor to river planform changes. Alternatively, tectonics could also have played an important role in controlling the river planform styles, since it can uplift the source area, introduce sediment into the system, and regulate stream style and process by influencing slope, sediment supply and even discharge (Kraus & Middleton, 1987). The Bighorn Basin was tectonically active during the Palaeocene and Eocene. The relatively constant basin subsidence rates (Abels *et al.*, 2013; Foreman, 2014) could suggest that climatic factors might have been more dominant, resulting in the alternation of river planform styles over certain timescales, although the influences of short-term tectonic fluctuations cannot be ruled out.

The early Eocene river systems in the Bighorn Basin experienced strong climate alternations likely driven by orbital forcing (Abels *et al.*, 2013), and these climate alternations may be embodied by changes in temperature, precipitation, vegetation cover, bank erodibility, suspended load/bedload ratio and seasonal contrast (Vandenberghe, 1995, 2003). It is anticipated that some other proxies may provide constraints for inference of the above-mentioned climate alternations, particularly the hydrodynamic conditions. However, sandbody data are not yet integrated with other proxies during the early Eocene, such as palaeosol data, in the Bighorn Basin studies to support palaeoclimatic reconstructions. Foreman (2014), however, has integrated sedimentological data with geochemical, palaeoichnological and palaeobotanical proxy records to characterize the climatic shift of Palaeocene–Eocene thermal maximum (PETM), providing interesting and inspiring insights. Therefore, a detailed stratigraphic analysis is needed to stratigraphically and statistically establish a possible precession-scale or eccentricity-scale relation between floodplain aggradational cycles (*cf.* Wang *et al.*, 2021) and channel sandstone bodies of different river planform styles to improve the climatic reconstruction in the Bighorn Basin.

CONCLUSIONS

In this study, a comprehensive sedimentological analysis is carried out on outcrops of the lower Eocene Willwood Formation in the McCullough Peaks area of the northern Bighorn Basin, USA, using both field-documented data and unmanned aerial vehicle (UAV)-photogrammetric model measurements. A total of four channel lithofacies associations are recognized, which are interpreted to be deposits of four river planform styles: crevasse channel, trunk channel, braided-like channel and sinuous-like channel, respectively, with the latter two styles as the dominant ones. Braided-like and sinuous-like channel sandstone bodies differ significantly in thicknesses, being on average 6.1 m versus 9.0 m, but they have similar widths of on average 231 m and palaeoflow directions of on average N 003°. They are different in lithofacies compositions and proportions, but planar cross-stratified sandstone is the most dominant lithofacies in both types of deposits. The alternating presence of sinuous and braided river styles recorded in the outcrop offers insights into the refined

reconstruction of a palaeogeographical model for the early Eocene period. In the schematized model, several transverse systems confluence with an axial system roughly following the basin axis in line with previous reconstructions. In addition to the importance for understanding the depositional patterns of the Bighorn Basin, this study efficiently synthesizes traditional sedimentological data collection often hampered by small sample sizes with UAV-based photogrammetry that can contribute to abundant data employment. This innovation is expected to provide a template for future data collection that can substantially increase the sample size of sedimentological studies so as to eliminate the data biases to a large extent.

ACKNOWLEDGEMENTS

This study was financially supported by TopSectors GeoEnergie, Equinor and Wintershall Noordzee to HAA, JEAS, AWM and TFB (FRESCO Project, Grant No. TKI2018–03–GE), China Scholarship Council to YW (No. 201606440046), the Dutch Molengraaff fund (Stichting Molengraaff Fonds) to YW, and the IAS/SEPM travel grant to YW. Scott Wing is thanked for constructive comments on the Bighorn Basin palaeogeomorphology. The authors acknowledge help from Chaowen Wang, Dirk-Jan Walstra and the Churchill family of Wyoming. An earlier version of this manuscript was significantly improved with the help of the Ph.D. committee members of YW, including Esther Stouthamer, Giovanni Bertotti, Gary Hampson, Klaudia Kuiper and Chris Fielding, as well as reviewers and editors of *Sedimentology*, including Amanda Owen, Sian Davies-Vollum, an anonymous reviewer, Editorial Office Manager Elaine Richardson, Associate Editor Chris Fielding and Chief Editor Piret Plink-Björklund.

CONFLICTS OF INTEREST

The authors declare no conflicts of interest in preparing this manuscript.

DATA AVAILABILITY STATEMENT

The data that support the findings of this study are available from the corresponding author upon request.

REFERENCES

Abdul Aziz, H., **Hilgen, F.J.**, **van Luijk, G.M.**, **Sluijs, A.**, **Kraus, M.J.**, **Pares, J.M.** and **Gingerich, P.D.** (2008) Astronomical climate control on paleosol stacking patterns in the upper Paleocene–lower Eocene Willwood formation, Bighorn Basin, Wyoming. *Geology*, **36**, 531.

Abels, H.A., **Clyde, W.C.**, **Gingerich, P.D.**, **Hilgen, F.J.**, **Fricke, H.C.**, **Bowen, G.J.** and **Lourens, L.J.** (2012) Terrestrial carbon isotope excursions and biotic change during Palaeogene hyperthermals. *Nature Geosci.*, **5**, 326–329.

Abels, H.A., **Kraus, M.J.** and **Gingerich, P.D.** (2013) Precession-scale cyclicity in the fluvial lower Eocene Willwood formation of the Bighorn Basin, Wyoming (USA). *Sedimentology*, **60**, 1467–1483.

Abels, H.A., **Lauretano, V.**, **van Yperen, A.E.**, **Hopman, T.**, **Zachos, J.C.**, **Lourens, L.J.**, **Gingerich, P.D.** and **Bowen, G.J.** (2016) Environmental impact and magnitude of paleosol carbonate carbon isotope excursions marking five early Eocene hyperthermals in the Bighorn Basin, Wyoming. *Clim. Past*, **12**, 1151–1163.

Allen, J.R.L. (1978) Studies in fluviatile sedimentation: an exploratory quantitative model for the architecture of avulsion-controlled alluvial suites. *Sediment. Geol.*, **21**, 129–147.

Allen, J.R.L. (1983) Studies in fluviatile sedimentation: bars, bar-complexes and sandstone sheets (low-sinuoisty braided streams) in the brownstones (L. Devonian) welshborders. *Sed. Geol.*, **33**, 237–293.

Allen, J.P., **Fielding, C.R.**, **Gibling, M.R.** and **Rygel, M.C.** (2013) Recognizing products of palaeoclimate fluctuation in the fluvial stratigraphic record: an example from the Pennsylvanian to lower Permian of Cape Breton Island, Nova Scotia. *Sedimentology*, **61**, 1332–1138.

Ashmore, P. (2013) 9.17 morphology and dynamics of braided rivers. In: *Treatise on Geomorphology* (Eds Shroder, J. and Wohl, E.), **9**, pp. 289–312. Academic Press, San Diego, CA.

Bettess, R. and **White, W.R.** (1983) Meandering and braiding of alluvial channels. *Proc. Inst. Civil Eng.*, **75**, 525–538.

Bijkerk, J.F., **ten Veen, J.**, **Postma, G.**, **Mikeš, D.**, **van Strien, W.** and **de Vries, J.** (2014) The role of climate variation in delta architecture: lessons from analogue modelling. *Basin Res.*, **26**, 351–368.

Birgenheier, L.P., **Berg, M.D.V.**, **Plink-Björklund, P.**, **Gall, R.D.**, **Rosencrans, E.**, **Rosenberg, M.J.**, **Toms, L.C.** and **Morris, J.** (2019) Climate impact on fluvial-lake system evolution, Eocene Green River Formation, Uinta Basin, Utah, USA. *GSA Bull.*, **132**, 562–587.

Blackstone, D.L. (1940) Structure of the Pryor Mountains Montana. *J. Geol.*, **48**, 590–618.

Bourquin, S., **Guillocheau, F.** and **Péron, S.** (2009) Braided rivers within an arid alluvial plain (example from the lower Triassic, western German Basin): recognition criteria and expression of stratigraphic cycles. *Sedimentology*, **56**, 2235–2264.

Bown, T.M. (1980) Summary of latest cretaceous and Cenozoic sedimentary, tectonic and erosional events, Bighorn Basin, Wyoming. In: *Early Cenozoic Paleontology and Stratigraphy of the Bighorn Basin, Wyoming* (Ed. Gingerich, P.D.), *Univ. Mich. Pap. Paleontol*, **24**, 25–32.

Bown, T.M. and **Kraus, M.J.** (1981) Lower Eocene alluvial paleosols (Willwood formation, Northwest Wyoming, U.S.A) and their significance for paleoecology,

paleoclimatology, and basin analyses. *Palaeogeogr. Palaeoclimatol. Palaeoecol.*, **34**, 1–30.

Bown, T.M. and **Kraus, M.J.** (1987) Integration of channel and floodplain suites, developmental sequence and lateral relations of alluvial paleosols. *J. Sediment. Petrol.*, **57**, 587–601.

Bradley, R.W. and **Venditti, J.G.** (2017) Reevaluating dune scaling relations. *Earth Sci. Rev.*, **165**, 356–376.

Braudrick, C.A., **Dietrich, W.E.**, **Leverich, G.T.** and **Sklar, L.S.** (2009) Experimental evidence for the conditions necessary to sustain meandering in coarse.Bedded rivers. *Proc. Natl. Acad. Sci.*, **106**, 16936–16941.

Bridge, J.S. (1993) The interaction between channel geometry, water flow, sediment transport and deposition in braided rivers. *Geol. Soc. Lond. Spec. Publ.*, **75**, 13–71.

Bridge, J.S. and **Leeder, M.R.** (1979) A simulation model of alluvial stratigraphy. *Sedimentology*, **26**, 617–644.

Bridge, J.S., **Smith, N.D.**, **Trent, F.**, **Gabel, S.L.** and **Bernstein, P.** (1986) Sedimentology and morphology of a low sinuosity river: Calamus River, Nebraska Sand Hills. *Sedimentology*, **33**, 851–870.

Bridge, J.S. and **Tye, B.** (2000) Interpreting the dimensions of ancient fluvial channel bars, channels, and channel belts from wireline-logs and cores. *AAPG Bulletin*, **84**, 1205–1228.

Bryant, I., **Carr, D.**, **Cirilli, P.**, **Drinkwater, N.**, **McCormick, D.**, **Tilke, P.** and **Thurmond, J.** (2000) Use of 3D digital analogues as templates in reservoir modelling. *Petroleum Geoscience*, **6**, 195–201.

Buckley, S.J., **Ringdal, K.**, **Naumann, N.**, **Dolva, B.**, **Kurz, T.H.**, **Howell, J.A.** and **Dewez, T.J.B.** (2019) LIME: software for 3-D visualization, interpretation, and communication of virtual geoscience models. *Geosphere*, **15**, 222–235.

Church, M. (2006) Bed material transport and the morphology of alluvial river channels. *Annu. Rev. Earth Planet. Sci.*, **34**, 325–354.

Clyde, W.C. and **Christensen, K.E.** (2003) Testing the relationship between pedofacies and avulsion using Markov analysis. *Am. J. Sci.*, **303**, 60–71.

Clyde, W., **Stamatakos, J.** and **Gingerich, P.** (1994) Chronology of the Wasatchian land-mammal age (early Eocene): magnetostratigraphic Results from the McCullough peaks section, northern Bighorn Basin, Wyoming. *J. Geol.*, **102**, 367–377.

Coleman, J.M. (1969) Brahmaputra river: channel processes and sedimentation. *Sediment. Geol.*, **3**, 129–239.

Colombera, L., **Arévalo, O.J.** and **Mountney, N.P.** (2017) Fluvial-system response to climate change: the Paleocene-Eocene Tremp group, Pyrenees, Spain. *Global Planet. Change*, **157**, 1–17.

Colombera, L., **Mountney, N.P.**, **Howell, J.A.**, **Rittersbacher, A.**, **Felletti, F.** and **McCaffrey, W.D.** (2016) A test of analog-based tools for quantitative prediction of large-scale fluvial architecture. *Bulletin*, **100**, 237–267.

Connell, S.D., **Kim, W.**, **Paola, C.** and **Smith, G.A.** (2012) Fluvial morphology and sediment-flux steering of axial-transverse boundaries in an Experimental Basin. *J. Sediment. Res.*, **82**, 310–325.

Davies, N.S. and **Gibling, M.R.** (2010) Cambrian to Devonian evolution of alluvial systems: the sedimentological impact of the earliest land plants. *Earth-Sci. Rev.*, **98**, 171–200.

Davies-Vollum, K.S. (1999) The formation of beds underlying carbonaceous shales as aquic paleosols: examples form the big Horn Basin of Wyoming. *Int. J. Coal Geol.*, **41**, 239–255.

Davies-Vollum, K.S. (2001) Not just red beds: the occurrence and formation of drab sections in the Willwood formation of the Bighorn Basin. In: *Paleocene-Eocene Stratigraphy and Biotic Change in the Bighorn and Clarks Fork Basins, Wyoming* (Ed. Gingerich, P.D.), **33**, 29–35. University of Michigan Papers on Paleontology.

Davies-Vollum, K.S. and **Kraus, M.J.** (2001) A relationship between alluvial backswamps and avulsion cycles: an example from the Willwood formation of the Bighorn Basin, Wyoming. *Sediment. Geol.*, **140**, 235–249.

Davies-Vollum, K.S. and **Wing, S.L.** (1998) Sedimentological, Taphonomic, and climatic aspects of Eocene swamp deposits (Willwood formation, Bighorn Basin, Wyoming). *PALAIOS*, **13**, 28.

DeCelles, P.G. and **Cavazza, W.** (1999) A comparison of fluvial megafans in the cordilleran (upper cretaceous) and modern Himalayan foreland basin systems. *Bull. Geol. Soc. Am.*, **111**, 1315–1334.

DeCelles, P.G., **Gray, M.B.**, **Ridgway, K.D.**, **Cole, R.B.**, **Pivnik, D.A.**, **Pequera, N.** and **Srivastava, P.** (1991) Controls on synorogenic alluvial-fan architecture, Beartooth conglomerate (Palaeocene), Wyoming and Montana. *Sedimentology*, **38**, 567–590.

Dickinson, W.R., **Klute, M.A.**, **Hayes, M.J.**, **Janecke, S.U.**, **Erik, R.**, **Mckittrick, M.A.**, **Olivares, M.D.**, **Klute, M.A.** and **Hayes, M.J.** (1988) Paleogeographic and paleotectonic setting of Laramide sedimentary basins in the central Rocky Mountain region. *Geol. Soc. Am. Bull.*, **100**, 1023–1039.

Enge, H.D., **Buckley, S.J.**, **Rotevatn, A.** and **Howell, J.A.** (2007) From outcrop to reservoir simulation model: workflow and procedures. *Geosphere*, **3**, 469.

Ethridge, F.G. and **Schumm, S.A.** (1978). Reconstructing paleochannel morphologic and flow characteristics: methodology, limitations, and assessment. In: *Fluvial Sedimentology* (Ed. Miall, A.D.), pp. 703–721. Canadian Society of Petroleum Geologists, Calgary, Alberta.

Fabuel-Perez, I., **Hodgetts, D.** and **Redfern, J.** (2009) A new approach for outcrop characterization and geostatistical analysis of a low-sinuosity fluvial-dominated succession using digital outcrop models: upper Triassic Oukaimeden sandstone formation, central high atlas, Morocco. *Am. Assoc. Petrol. Geol. Bulletin*, **93**, 795–827.

Fielding, C.R. (1986) Fluvial channel and overbank deposits from the Westphalian of the Durham coalfield, NE England. *Sedimentology*, **33**, 119–140.

Fielding, C.R. (2006) Upper flow regimes sheets, lenses and scour fills: extending the range of architectural elements for fluvial sediment bodies. *Sedim. Geol.*, **190**, 227–240.

Fielding, C.R., **Alexander, J.** and **Allen, J.P.** (2018) The role of discharge variability in the formation and preservation of alluvial sediment bodies. *Sediment. Geol.*, **365**, 1–20.

Finn, T.M., **Kirschbaum, M.A.**, **Roberts, S.B.**, **Condon, S.M.**, **Roberts, L.N.R.**, and **Johnson, R.C.** (2010) Cretaceous–tertiary composite Total petroleum system (503402), Bighorn Basin, Wyoming and Montana. *U.S. Geological Survey Digital Data Series DDS-69-V*, 157 p.

Fisher, J.A., **Nichols, G.J.** and **Waltham, D.A.** (2007) Unconfined flow deposits in distal sectors of fluvial distributary systems: examples from the Miocene Luna and Huesca systems, northern Spain. *Sediment. Geol.*, **195**, 55–73.

Foose, R.M., **Wise, D.U.** and **Garbarini, G.S.** (1961) Structural geology of the Beartooth Mountains, Montana and Wyoming. *Geol. Soc. Am. Bull.*, **72**, 1143.

Foreman, B.Z. (2014) Climate-driven generation of a fluvial sheet sand body at the Paleocene-Eocene boundary in north-West Wyoming (USA). *Basin Res.*, **26**, 225–241.

Foreman, B.Z., **Heller, P.L.** and **Clementz, M.T.** (2012) Fluvial response to abrupt global warming at the Palaeocene/Eocene boundary. *Nature*, **491**, 92–95.

Friend, P.F. (1983) Towards the field classification of an alluvial architecture or sequence. In: *Modern and Ancient Fluvial Systems* (Eds Collinson, J.D. and Lewin, J.), *IAS Spec. Publ*, **6**, 345–354.

Ghinassi, M. and **Ielpi, A.** (2015) Stratal architecture and morphodynamics of downstream migrating fluvial point bars (Jurassic Scalby formation, UK). *J. Sed. Res.*, **85**, 1123–1137.

Ghinassi, M. and **Ielpi, A.** (2018) Morphodynamics and facies architecture of streamflow-dominated, sand-rich alluvial fans, Pleistocene upper Valdarno Basin, Italy. *Geol. Soc. Lond. Spec. Publ.*, **440**, 175–200.

Ghinassi, M., **Ielpi, A.**, **Aldinucci, M.** and **Fustic, M.** (2016) Downstream-migrating fluvial point bars in the rock record. *Sediment. Geol.*, **334**, 66–96.

Ghinassi, M., **Nemec, W.**, **Aldinucci, M.**, **Nehyba, S.**, **Özaksoy, V.** and **Fidolini, F.** (2014) Plan-form evolution of ancient meandering rivers reconstructed from longitudinal outcrop sections. *Sedimentology*, **61**, 952–977.

Gibling, M.R. (2006) Width and thickness of fluvial channel bodies and valley fills in the geological record: a literature compilation and classification. *J. Sediment. Res.*, **76**, 731–770.

Gibling, M.R. and **Davies, N.S.** (2012) Palaeozoic landscapes shaped by plant evolution. *Nat. Geosci.*, **5**, 99–105.

Giles, P., **Whitehouse, B.** and **Karymbalis, E.** (2016) Interactions between alluvial fans and axial rivers in Yukon, Canada and Alaska, USA. In: *Geology and Geomorphology of Alluvial and Fluvial Fans: Terrestrial and Planetary Perspectives* (Eds Ventra, D. and Clarke, L.E.), *Geological Society, London, Special Publications*, **440**, 23–43.

Gingerich, P.D. (1983) Paleocene-Eocene faunal zones and a preliminary analysis of Laramide structural deformation in the Clark's Fork Basin, Wyoming. In 34th Annual Field Conference, *Wyoming Geological Association Guidebook*, pp. 185–195.

Gingerich, P.D. (2010) Mammalian faunal succession through the Paleocene-Eocene thermal maximum (PETM) in western North America. *Vertebrata PalAsiatica*, **48**, 308–327.

Gradstein, F.M., **Ogg, J.G.**, **Schmitz, M.D.** and **Ogg, G.M.** (2012) *The Geologic Time Scale 2012*. Elsevier, Amsterdam.

Gries, R. (1983) North-south compression of Rocky Mountain foreland structures. In: *Rocky Mountain Foreland Basins and Uplifts* (Ed. Lowell, J.D.), pp. 9–32. Rocky Mountain Association of Geologists, Denver, CO.

Hajek, E.A., **Heller, P.L.** and **Sheets, B.A.** (2010) Significance of channel-belt clustering in alluvial basins. *Geology*, **38**, 535–538.

Hampson, G.J., **Jewell, T.O.**, **Irfan, N.**, **Gani, M.R.** and **Bracken, B.** (2013) Modest change in fluvial style with varying accommodation in regressive alluvial-to-coastal-plain wedge: upper cretaceous Blackhawk formation, Wasatch plateau, Central Utah, U.S.A. *J. Sediment. Res.*, **83**, 145–169.

Harms, J.C. and **Fahnestock, R.K.** (1965) Stratification, bed forms and flow phenomena (with an example from the Rio Grande). In: *Primary Sedimentary Structures and their Hydrodynamics Interpretation* (Ed. Middleton, G.V.), *Soc. Econ. Paleontol. Mineral., Spec. Publ*, **12**, 84–115.

Hartley, A.J., **Owen, A.**, **Swan, A.**, **Weissmann, G.S.**, **Holzweber, B.I.**, **Howell, J.**, **Nichols, G.** and **Scuderi, L.** (2015) Recognition and importance of amalgamated sandy meander belts in the continental rock record. *Geology*, **43**, 679–682.

Hartley, A.J., **Owen, A.**, **Weissmann, G.S.** and **Scuderi, L.A.** (2018) Modern and Ancient Amalgamated Sandy Meander-Belt Deposits: Recognition and Controls on Development. In: *Fluvial Meanders and their Sedimentary Products in the Rock Record* (Eds. Ghinassi, M., Colombera, L., Mountney, N.P., Reesink, A.J.H. and Bateman, M.), pp. 349–383. International Association of Sedimentologists, Oxford.

Holbrook, J.M. and **Allen, S.D.** (2021) The case of the braided river that meandered: Bar assemblages as a mechanism for meandering along the pervasively braided Missouri River, USA. *GSA Bull.*, **133**, 1505–1530.

Holbrook, J., **Scott, R.W.** and **Oboh-Ikuenobe, F.E.** (2006) Base-level buffers and buttresses: a model for upstream versus downstream control on fluvial geometry and architecture within sequences. *J. Sediment. Res.*, **76**, 162–174.

Howell, J.A., **Martinius, A.W.** and **Good, T.R.** (2014) The application of outcrop analogues in geological modelling: a review, present status and future outlook. *Geol. Soc. Lond. Spec. Publ.*, **387**, 1–25.

Hoy, R.G. and **Ridgway, K.D.** (1997) Structural and sedimentological development of footwall growth synclines along an intraforeland uplift, east-Central Bighorn Mountains, Wyoming. *Geol. Soc. Am. Bull.*, **109**, 915–935.

Jerolmack, D.J. and **Paola, C.** (2007) Complexity in a cellular model of river avulsion. *Geomorphology*, **91**, 259–270.

Karssenberg, D. and **Bridge, J.S.** (2008) A three-dimensional numerical model of sediment transport, erosion and deposition within a network of channel belts, floodplain and hill slope: extrinsic and intrinsic controls on floodplain dynamics and alluvial architecture. *Sedimentology*, **55**, 1717–1745.

Kennedy, J.F. (1969) The formation of sediment ripples, dunes and antidunes. *Annu. Rev. Fluid Mech.*, **1**, 147.

Kim, W., **Connell, S.D.**, **Steel, E.**, **Smith, G.A.** and **Paola, C.** (2011) Mass-balance control on the interaction of axial and transverse channel systems. *Geology*, **39**, 611–614.

Kraus, M.J. (1980) Genesis of a fluvial sheet sandstone, Willwood formation, Northwest Wyoming. *Univ. Michigan Pap. Paleontol.*, **24**, 87–94.

Kraus, M.J. (1983) *Genesis of Early Tertiary Exotic Metaquartzite Conglomerates in the Western Bighorn Basin, Northwest Wyoming*. PhD Thesis. University of Colorado, Boulder, CO.

Kraus, M.J. (1984) Sedimentology and tectonic setting of early tertiary quartzite conglomerates, Northwest Wyoming. In: *Sedimentology of Gravels and Conglomerates* (Eds Koster, E.H. and Steel, R.J.), *Canadian Society of Petroleum Geologists Memoir*, **10**, 203–216.

Kraus, M.J. (1985) Early tertiary quartzite conglomerates of the Bighorn Basin and their significance for paleogeographic reconstruction of northwest Wyoming. In: *Cenozoic Paleogeography of West-central United States* (Eds Flores, R.M. and Kaplan, S.S.), *Rocky Mountain Section of the Society for SEPM*, 71–91.

Kraus, M.J. (1987) Integration of channel and floodplain suites, II vertical relations of alluvial paleosols. *J. Sediment. Petrol.*, **57**, 602–612.

Kraus, M.J. (1996) Avulsion deposits in lower eocene alluvial rocks, Bighorn Basin, Wyoming. *J. Sediment. Res.*, **66**, 354–363.

Kraus, M.J. (1999) Paleosols in clastic sedimentary rocks: their geologic applications. *Earth-Sci. Rev.*, **47**, 41–70.

Kraus, M.J. (2002) Basin-scale changes in floodplain Paleosols: implications for interpreting alluvial architecture. *J. Sediment. Res.*, **72**, 500–509.

Kraus, M.J. and **Aslan, A.** (1993) Eocene hydromorphic Paleosols: significance for interpreting ancient floodplain processes. *J. Sediment. Petrol.*, **63**, 453–463.

Kraus, M.J. and **Bown, T.M.** (1993) Palaeosols and sandbody prediction in alluvial sequences. In: *Characterisation of Fluvial and Aeolian Reservoirs* (Eds North, C.P. and Prosser, D.J.), *Geol. Soc. London Spec. Publ*, **73**, pp. 23–31.

Kraus, M.J. and **Davies-Vollum, K.S.** (2004) Mudrock-dominated fills formed in avulsion splay channels: examples from the Willwood formation, Wyoming. *Sedimentology*, **51**, 1127–1144.

Kraus, M.J. and **Gwinn, B.** (1997) Facies and facies architecture of Paleogene floodplain deposits, Willwood formation, Bighorn Basin, Wyoming, USA. *Sediment. Geol.*, **114**, 33–54.

Kraus, M.J. and **Hasiotis, S.T.** (2006) Significance of different modes of rhizolith preservation to interpreting paleoenvironmental and paleohydrologic settings: examples from Paleogene paleosols, Bighorn Basin, Wyoming, U.S.A. *J. Sediment. Res.,* **76**, 633–646.

Kraus, M.J. and **Middleton, L.** (1987) Contrasting architecture of two alluvial suites in different structural settings. In: *Recent Developments in Fluvial Sedimentology* (Eds Ethridge, F.G., Fiores, R.M. and Harvey, M.D.), *SEPM Spec. Pub*, **39**, 253–262.

Kraus, M.J. and **Wells, T.M.** (1999) Recognizing avulsion deposits in the ancient stratigraphical record. In: *Fluvial Sedimentology VI* (Eds Smith, N.D. and Rogers, J.), *IAS Spec.Publ*, **28**, 261–268.

Leclair, S.F. and **Bridge, J.S.** (2001) Quantitative interpretation of sedimentary structures formed by river dunes. *J. Sediment. Res.*, **71**, 713–716.

Leopold, L.B. and **Wolman, M.G.** (1957) River channel patterns: braided, meandering and straight. *US Geol. Survey Prof. Paper*, **282-B**, 85.

Lillegraven, J.A. (2009) Where was the western margin of northwestern Wyoming's Bighorn Basin late in the early Eocene? In: *Papers on Geology, Vertebrate Paleontology, and Biostratigraphy in Honor of Michael O. Woodburne* (Ed. Albright, L.B., III), *Mus. Northern Arizona Bull*, **65**, 37–82.

Lillegraven, J.A. and **Ostresh, L.M., Jr.** (1988) Evolution of Wyoming's early Cenozoic topography and drainage patterns. *Nat. Geogr. Res.*, **4**, 303–327.

Limaye, A.B. (2020) How do braided rivers grow channel belts? *J. Geophys. Res. Earth*, **125**, e2020JF005570.

Lorenz, J.C. and **Nadon, G.C.** (2002) Braided-river deposits in amuddy depositional setting: the Molina member of the Wasatch formation (Paleogene) west-Central Colorado, U.S.A. *J. Sedim. Res.*, **72**, 376–385.

Mackey, S.D. and **Bridge, J.S.** (1995) Three-dimensional model of alluvial stratigraphy: theory and application. *J. Sediment. Res.*, **65**, 7–31.

Malone, D.H., **Craddock, J.P.**, **Link, P.K.**, **Foreman, B.Z.**, **Scroggins, M.A.** and **Rappe, J.** (2017) Detrital zircon geochronology of quartzite clasts, Northwest Wyoming: implications for cordilleran Neoproterozoic stratigraphy and depositional patterns. *Precambrian Res.*, **289**, 116–128.

McBride, E.F. (1963) A classification of common sandstones. *J. Sed. Petrol.*, **33**, 664–669.

van der Meulen, B., **Gingerich, P.D.**, **Lourens, L.J.**, **Meijer, N.**, **van Broekhuizen, S.**, **van Ginneken, S.** and **Abels, H.A.** (2020) Carbon isotope and mammal recovery from extreme greenhouse warming at the Paleocene–Eocene boundary in astronomically-calibrated fluvial strata, Bighorn Basin, Wyoming, USA. *Earth Planet. Sci. Lett.*, **534**, 116044.

Miall, A.D. (1985) Architectural-element analysis: a new method of facies analysis applied to fluvial deposits. *Earth Sci. Rev.*, **22**, 261–308.

Miall, A.D. (1994) Reconstructing fluvial macroform architecture from two-dimensional outcrops: examples from the Castlegate sandstone, book cliffs, Utah. *J. Sediment. Res.*, **64**, 146–158.

Miall, A.D. (1996) *The Geology of Fluvial Deposits (Sedimentrary Facies. Basin Analysis, and Petroleum Geology)*. Springer-verlag, New York, NY, 565 p.

Muto, T., **Steel, R.** and **Swenson, J.** (2007) Autostratigraphy: a framework norm for genetic stratigraphy. *J. Sediment. Res.*, **77**, 2–12.

Neasham, J.W. (1967) *The Stratigraphy of the Willwood Formation in the Vicinity of Sheep Mountain, Southwestern Bighorn County, Wyoming*. Master Thesis. Iowa State University, Ames, IA, 74 p.

Neasham, J.W. (1970) *Sedimentology of the Willwood Formation (Lower Eocene): An Alluvial Molasse Facies in Northwestern Wyoming*. PhD Thesis. Iowa State University, Ames, IA, 98 p.

Neasham, J.W. and **Vondra, C.F.** (1972) Stratigraphy and petrology of the lower Eocene Willwood formation, Bighorn Basin, Wyoming. *Geol Soc America Bull*, **83**, 2167.

Owen, A., **Ebinghaus, A.**, **Hartley, A.J.**, **Santos, M.G.M.** and **Weissmann, G.S.** (2017) Multi-scale classification of fluvial architecture: an example from the Palaeocene-Eocene Bighorn Basin, Wyoming. *Sedimentology*, **64**, 1572–1596.

Owen, A., **Hartley, A.J.**, **Ebinghaus, A.**, **Weissmann, G.S.** and **Santos, M.G.M.** (2019) Basin-scale predictive models of alluvial architecture: constraints from the Palaeocene-Eocene, Bighorn Basin, Wyoming, USA. *Sedimentology*, **66**, 736–763.

Paredes, J.M., **Foix, N.N.** and **Allard, J.O.** (2016) Sedimentology and alluvial architecture of the bajo Barreal formation (upper cretaceous) in the Golfo San Jorge Basin: outcrop analogues of the richest oil-bearing fluvial succession in Argentina. *Mar. Petrol. Geol.*, **72**, 317–335.

Plink-Björklund, P. (2015) Morphodynamics of rivers strongly affected by monsoon precipitation: review of depositional style and forcing factors. *Sediment. Geol.*, **323**, 110–147.

Posamentier, H., **Davies, R.**, **Cartwright, J.** and **Wood, L.** (2007) Seismic geomorphology - an overview. *Geol. Soc. Lond. Spec. Publ.*, **277**, 1–14.

Pryor, W.A. (1960) Cretaceous sedimentation in upper Mississipi embayment. *AAPG Bulletin*, **44**, 1473–1504.

Sambrook Smith, G.H., **Ashworth, P.J.**, **Best, J.L.**, **Woodward, J.** and **Simpson, C.J.** (2006) The

sedimentology and alluvial architecture of the sandy braided South Saskatchewan River, Canada. *Sedimentology*, **53**, 413–434.

Santos, M.G.M., **Mountney, N.P.** and **Peakall, J.** (2016) Tectonic and environmental controls on Palaeozoic fluvial environments: reassessing the impacts of early land plants on sedimentation. *J. Geol. Soc. London*, **174**, 393–404.

Schumm, S.A. (1985) Patterns of alluvial rivers. *Annu. Rev. Earth Planet. Sci.*, **13**, 5–27.

Scotese, C., **Song, H.**, **Mills, B.** and **Meer, D.** (2021) Phanerozoic paleotemperatures: the Earth's changing climate during the last 540 million years. *Earth Sci. Rev.*, **215**, 103503. https://doi.org/10.1016/j.earscirev.2021.103503.

Secord, R., **Wing, S.** and **Chew, A.** (2008) Stable isotopes in early Eocene mammals as indicators of Forest canopy structure and resource partitioning. *Paleobiology*, **34**, 282–300.

Seeland, D. (1998) Late Cretaceous, Paleocene, and Early Eocene Paleogeography of the Bighorn Basin and Northwestern Wyoming. In *Cretaceous and Lower Tertiary Rocks of the Bighorn Basin, Wyoming and Montana; 49th Annual Field Conference Guidebook*, pp. 1–29.

Shanley, K.W. and **McCabe, P.J.** (1994) Perspectives on the sequence stratigraphy of continental strata. *AAPG Bulletin*, **78**, 544–568.

Smedes, H.W. and **Prostka, H.J.** (1972) Stratigraphic framework of the Absaroka volcanic supergroup in the Yellowstone National Park region. *U.S. Geol. Surv. Prof. Pap.*, **729-C**, 33.

Soil Survey Division Staff (1993) *Soil Survey Manual*, Vol. **18**. Soil Conservation Service, U.S. Department of Agriculture.

Summerfield, M.A. (1991) Tectonic geomorphology. *Prog. Phys. Geogr. Earth Environ.*, **15**, 193–205.

Sundell, K.A. (1990) Sedimentation and tectonics of the Absaroka Basin of northwestern Wyoming. In: Wyoming Sedimentation and Tectonics, *41st Annual Field Conference Guidebook*, 105–122.

Syzdek, J., **Malone, D.** and **Craddock, J.** (2019) Detrital zircon U-pb geochronology and provenance of the Sundance formation, Western Powder River Basin, Wyoming. *Mt. Geol.*, **56**, 295–317.

van den Berg, J.H., **Martinius, A.W.** and **Houthuys, R.** (2017) Breaching-related turbidites in fluvial and estuarine channels: examples from outcrop and Core and implications to reservoir models. *Marine Petrol. Geol.*, **82**, 178–205.

van de Lageweg, W.I., **Schuurman, F.**, **Cohen, K.**, **Van Dijk, W.**, **Shimizu, Y.** and **Kleinhans, M.** (2015) Preservation of meandering river channels in uniformly aggrading channel belts. *Sedimentology*, **63**, 586–608.

van Houten, F.B. (1944) Stratigraphy of the Willwood and Tatman formations in northwestern Wyoming. *Geol. Soc. Amer. Bull.*, **55**, 165–210.

Vandenberghe, J. (1995) Timescales, climate and river development. *Quatern. Sci. Rev.*, **14**, 631–638.

Vandenberghe, J. (2003) Climate forcing of fluvial system development: an evolution of ideas. *Quatern. Sci. Rev.*, **22**, 2053–2060.

Vandenberghe, N., **Hilgen, F.J.** and **Speijer, R.P.** (2012) The Paleogene period. In: *The Geologic Time Scale 2012* (Eds Gradstein, F.M., Ogg, J.G., Schmitz, M. and Ogg, G.), pp. 855–921. Elsevier, Amsterdam.

Wang, C., **Adriaens, R.**, **Hong, H.**, **Elsen, J.**, **Vandenberghe, N.**, **Lourens, L.J.**, **Gingerich, P.D.** and **Abels, H.A.** (2017) Clay mineralogical constraints on weathering in response to early Eocene hyperthermal events in the Bighorn Basin, Wyoming (Western interior, USA). *Geol. Soc. Am. Bull.*, **129**, 997–1011.

Wang, Y., **Baars, T.**, **Storms, J.**, **Martinius, A.**, **Gingerich, P.**, **Chmielewska, M.**, **Buckley, S.** and **Abels, H.** (2021) Spatial characteristics and kinematics of precession-driven floodplain aggradation cycles in the lower Eocene Willwood formation of the Bighorn Basin, Wyoming, USA. *Eartharxiv* https://doi.org/10.31223/X5931M.

Wang, Y., **Storms, J.E.A.**, **Martinius, A.W.**, **Karssenberg, D.** and **Abels, H.A.** (2021) Evaluating alluvial stratigraphic response to cyclic and non-cyclic upstream forcing through process-based alluvial architecture modelling. *Basin Res.*, **33**, 48–65.

Weissmann, G.S., **Hartley, A.J.**, **Scuderi, L.A.**, **Nichols, G.J.**, **Owen, A.**, **Wright, S.**, **Felicia, A.L.**, **Holland, F.** and **Anaya, F.M.L.** (2015) Fluvial geomorphic elements in modern sedimentary basins and their potential preservation in the rock record: a review. *Geomorphology*, **250**, 187–219.

Went, D.J. and **McMahon, W.J.** (2018) Fluvial products and processes before the evolution of land plants: evidence from the lower Cambrian series rouge, English Channel region. *Sedimentology*, **65**, 2559–2594.

Westerhold, T., **Marwan, N.**, **Drury, A.J.**, **Liebrand, D.**, **Agnini, C.**, **Anagnostou, E.**, **Barnet, J.S.K.**, **Bohaty, S.M.**, **De Vleeschouwer, D.**, **Florindo, F.**, **Frederichs, T.**, **Hodell, D.A.**, **Holbourn, A.E.**, **Kroon, D.**, **Lauretano, V.**, **Littler, K.**, **Lourens, L.J.**, **Lyle, M.**, **Pälike, H.**, **Röhl, U.**, **Tian, J.**, **Wilkens, R.H.**, **Wilson, P.A.** and **Zachos, J.C.** (2020) An astronomically dated record of Earth's climate and its predictability over the last 66 million years. *Science*, **369**, 1383–1387.

Williams, G.P. (1986) River meanders and channel size. *J. Hydrol.*, **88**, 147–164.

Willis, B.J. and **Behrensmeyer, A.K.** (1995) Fluvial systems in the Siwalik Miocene and Wyoming Paleogene. *Palaeogeogr. Palaeoclimatol. Palaeoecol.*, **115**, 13–35.

Willis, J.B. and **Tang, H.** (2010) Three-dimensional connectivity of point-bar deposits. *J. Sediment. Res.*, **80**, 440–454.

Wilson, C.W. (1936) Geology of the nye-bowler linement, Stillwater and carbon counties, Montana. *Am. Assoc. Petrol. Geol. Bull.*, **20**, 1161–1188.

Wing, S. and **Bown, T.M.** (1985) Fine scale reconstruction of late Paleocene-early Eocene paleogeography in the Bighorn Basin of northern Wyoming. In: *Cenozoic paleogeography of the west-central United States: Rocky Mountain Section* (Eds Flores, R. and Kaplan, S.), *Society of Economic Paleontologists and Mineralogists*, 93–105.

Wise, D.U. (2000) Laramide structures in basement and cover of the Beartooth uplift near red lodge, Montana. *AAPG Bulletin*, **84**, 360–375.

Yonkee, W.A. and **Weil, A.B.** (2015) Tectonic evolution of the Sevier and Laramide belts within the north American cordillera orogenic system. *Earth-Sci. Rev.*, **150**, 531–593.

Yuretich, R.F., **Hickey, L.J.**, **Gregson, B.P.** and **Hsia, Y.L.** (1984) Lacustrine deposits in the Paleocene fort union formation, northern Bighorn Basin, Montana. *J. Sed. Petrol.*, **54**, 836–852.

Zachos, J.C., **McCarren, H.**, **Murphy, B.**, **Röhl, U.** and **Westerhold, T.** (2010) Tempo and scale of late Paleocene and early Eocene carbon isotope cycles: implications for the origin of hyperthermals. *Earth Planet. Sci. Lett.*, **299**, 242–249.

Manuscript received 17 July 2021; revision accepted 6 July 2022

Supporting Information

Additional information may be found in the online version of this article:

Fig. S1. (A) to (D) Four examples showing how widths of braided-like channel sandstone bodies are measured. (E) to (H) Four examples showing how widths of sinuous-like channel sandstone bodies are measured. The black dots indicate the presence of the sandstone body at the outcrop surface, and two dashed boundary lines are along the average palaeoflow direction (N004°). A sinuosity index is calculated in subfigure (H), indicated by the red dot line. Locations of DCA, PB and UDC sections can be found in Fig. 2 for comparison.

Fig. S2. Petrographic characteristics of braided-like and sinuous-like channel sandstone deposits. (A) and (B) Thin sections of braided-like channel sandstone deposits under plane-polarized and orthogonally-polarized light. (C) and (D) Thin sections of sinuous-like channel sandstone deposits under plane- and orthogonally-polarized light. B = biotite; C = chert; M = microline; P = plagioclase; Q = quartz. White bar for scale is 500 μm.

Table S1. Presence of lithofacies in each facies association.

